CFD Based Estimation of Wind Energy Potential in Urban Locations

Anahita Ghassemi Panah

A Thesis

In the Department

Of

Mechanical, Industrial & Aerospace Engineering

Presented in the Partial Fulfillment of Requirements for the Degree of

Master of applied science (mechanical engineering)

at

Concordia University

Montréal, Québec, CANADA

August 2021

CONCORDIA UNIVERSITY

School of Graduate Studies

This is to certify that the thesis prepared

By: Anahita Ghassemi Panah

Entitled: CFD based estimation of wind energy potential in urban locations

And submitted in partial fulfillment of the requirements for the degree of

Master of Applied Science (Mechanical Engineering)

complies with the regulation of the University and meets the accepted standards with respect to originality and quality.

Signed by the final Examining Committee:

_____ Chair

Mojtaba Kheiri

_____ Examiner

Mojtaba Kheiri

_____ Examine

Ted Stathopoulos

_____ Supervisor

Marius Paraschivoiu

Approved by: _____

Dr. Mamoun Medraj, Graduate Program Director

Department of Mechanical and Industrial Engineering

_____

Mourad Debbabi, Ph.D., Dean

Dean, Faculty of Engineering and Computer Science (ENCS)

Abstract

CFD Based Estimation of Wind Energy Potential in Urban Locations

Anahita Ghassemi Panah

Wind energy plays a critical role as a safe and clean source of energy. However, the complexity of wind patterns produced by the topographical characteristics of urban environments considerably affect the performance of urban wind turbines. In order to address these effects, this study utilizes both Computational Fluid Dynamics (CFD) and meteorological data in order to simulate the wind flow in an urban area and to predict the performance of a wind turbine at specific locations on top of buildings. This thesis presents a review of vertical axis wind turbines and the desirable locations of these types of wind turbines above a building in an urban area. Numerical simulations offer a cost-effective method with an acceptable accuracy to evaluate wind turbine locations. Two test cases have been studied to illustrate the behavior of wind turbines located on the roofs of buildings. The full scale of the urban area and the computational domain are constructed, and the flow is simulated based on the STAR CCM+ ® software. The three-dimensional, steady Reynolds-Averaged Navier-Stokes equations are solved to obtain the velocity of the wind in urban areas. Meteorological data is then used to estimate the potential energy production at specific locations on the top of a building. Multiple locations are studied in terms of annual total Energy output to find out the best potential position for turbine installation. Results demonstrate a significant difference of energy output for different locations of the wind turbines on the same building. This study introduces an effective tool to study the annual total energy output potential at multiple locations above the building in much shorter time span (within a month) rather than the existing experimental or field methods.

Keywords: Roof Mounted Wind Turbines, Urban Area, CFD, STAR CCM+, Wind Profile, Total Energy Output**.**

Acknowledgments

Table of Contents

List of Figures

List of Tables

NOMENCLATURE

Cd	=	Coefficient of drag
Cpower	=	Power coefficient
Cp	=	Pressure Coefficient
HAWT	=	Horizontal axis wind turbine
L	=	Characteristic length (m)
Pwind	=	Wind power (W)
Re	=	Reynolds number
TSR	=	Tip speed ratio
U	=	Wind speed (m/s)
UABL	=	Atmospheric boundary layer wind speed (m/s)
U∞	=	Free stream velocity (m/s)
Uref	=	Reference wind velocity for the simulations [m/s]
Ucp	=	Wind velocity calculated at control points [m/s]
Uwind	=	Wind velocity data from meteorological statistics [m/s]
Uactual	=	Estimated wind velocity at turbine rotor [m/s]
VAWT	=	Vertical axis wind turbine
y	=	Coordinate value (m)
y+	=	Mesh y plus value
Δy	=	Wall first layer mesh height (m)
z_0	=	Aerodynamic roughness
ρ	=	Air density (kg/m3)
ω	=	Angular velocity (rad/s)
ν	=	Kinematic Viscosity (m2/s)

κ = Von Karman constant

K = Turbulent kinetic energy (m2/s2)

ε = Turbulent dissipation (m2/s2)

CHAPTER 1: Introduction

The use of wind as a source of energy goes back to 10th century in Persia and 13th century in China[1]. Wind was considered as a source of energy for sail ships, mill grain and pumping the water. Windmills and watermills were two sources of producing energy before steam engine was invented. Currently, Wind energy is known as a clean energy which is renewable, widely distributed, and available. It is a viable alternative to fossil fuels with no greenhouse gas emission. To benefit from this source of energy, generally vast wind turbine plants are placed together in an area called a wind farm. However, recently, interest has grown to supply localized clean power in urban and suburban areas rather than generalized wide wind-power plants. Generally Horizontal Axis Wind Turbines (HAWT) are more common in wind-power plants while Vertical Axis Wind Turbines (VAWT) are more interesting in urban areas or offshore. Figure 1 and Figure 2 show the structure of both HAWT and VAWT.

Figure 1: The Horizontal Axis Wind Turbine (HAWT)[2]
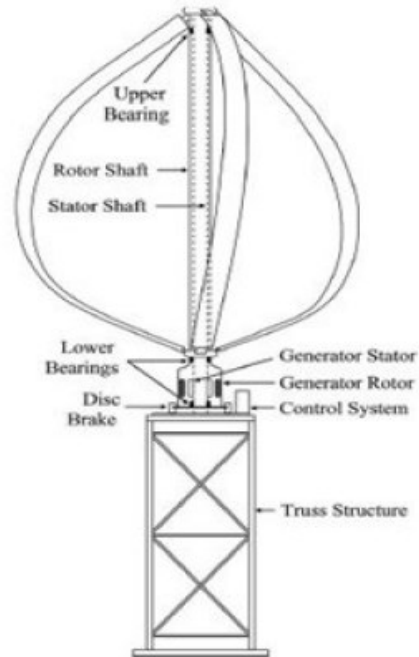
Figure 2: a) Vertical Axis Wind Turbine (VAWT) b) The schematic of different parts in a typical VAWT

1.1 Urban wind energy

The investigation of wind around buildings in urban areas plays a crucial role in many applications such as wind energy and power generation, air pollution, pedestrian comfort and natural ventilation deigns [3]. With the rise in industrialization and the public awareness about the global warming and alternative methods for moderating the fossil fuel consumption, wind energy in urban areas is becoming more interesting. Wind energy has shown an exponentially higher replacement interest among other alternatives for fossil fuels (such as solar, hydro, tidal and geothermal). In the first fifteen years of the twenty first century, the implementations of wind turbines have increased by 2000 times [4]. Today, due to growing demand for clean, renewable, and safe energy, the roof mounted wind turbines attract a considerable attention as they are a clean energy source with easy installation in urban areas.

1.2 Urban wind turbines

Exploring roof mounted wind turbines can lead to developing cost effective energy as an alternative method for reducing the consumption of fossil fuels and the emission of greenhouse gases. Moreover, the roof mounted wind turbines in urban areas could result into an efficient and low cost associated with wind power by producing the energy in the closest possible location to where it is utilized, at the top of residential buildings [5]. Although most of the developments in both technology and manufacturing infrastructures, have been achieved in fields far from the urban area, there is a considerable potential of wind energy in urban areas around the high-rise buildings, near the railway tracks etc. Furthermore, the Horizontal Axis Wind Turbines (HAWT) are less attractive to residents due to their noise, aesthetic, visual and safety public concerns. Vertical Axis Wind Turbines (VAWT) seems to be a suitable alternative as these turbines are less noisy and more visually pleasant and could be installed on the roof of high-rise buildings in urban areas [6]. Although the vertical roof mounted wind turbines generally demonstrated acceptable rates of energy potential, the exact location of wind turbine must be analyzed due to the turbulence and unsteady wind flows above the buildings in urban areas. Since the successful operation of the wind turbine will happen in the best and specific location of the roof top of the high-rise buildings, the inaccurate analyze which leads to the wrong location for the installation of the turbine, could lead to the low performance.

1.3 Recent achievements on studying and analyzing the wind energy

Noticeable progresses have been made recently on topics related to exploiting wind energy and assessment of wind resources specially in urban areas, the selection and design of suitable wind turbines and the crucial role of aerodynamics and building constructions in enhancing the extraction mechanisms [7].

Due to some important difficulties of installing a wind turbine on a roof top of a building such as structural concerns and city bylaws regulations, some researchers have studied the implantation of wind turbines, specifically the challenges of installation an actual wind turbine in urban locations [8]. The current literature is more focused on the conventional wind turbines installed on the roof tops, however, the location of the building might reduce the efficiency of the generator [9], [10]. Due to the interest of governments for generating electrical energy from renewable resources, intensive efforts have been made on installation and performance assessment of micro wind turbines above buildings [11], although there are many challenges related to structural stability and respecting noise standards.

One of the advantages of wind flow in urban areas is that the wind speed near tall buildings at specific corners could be considerable, moreover, the produced energy at the roof tops of a city could be consumed locally. In wind energy generation, a small increase in wind speed could result in a significant rise in energy generation since in the generated power is a function of the cube of the wind speed [7].

Meteorological stations could provide the measured data of wind resources, but to assess such data in the specific locations, some methods should be used. The most popular direct methods are the Weibull and Rayleigh which are mathematical functions [12] which seems to have the most effectiveness in areas with high amounts of mean wind velocity such as offshores [13], and wind atlas data [14]. This statistical method can be apply for the evaluation of the wind speed characteristics and wind power at a specific height above the ground using average hourly data, There are some indirect methods such as numerical simulations with Computational Fluid Dynamics or wind tunnel experiments [15]. In addition, there has been studies on the effect of the architecture of building associated with height and roof shape and wind direction on the efficiency of energy production [13][16], and presenting an analysis on estimated potential energy of a wind regime [17].

The behavior of wind in urban areas is known as a complicated phenomenon, There have been some research efforts related to evaluating the environment and the location for extracting wind energy as well as field studies on installation of micro-wind turbines on urban structures [2], while

4

other projects were focusing on technical aspects of wind turbines such as wind turbine design [18], [19] and numerical simulations of the urban sites [20],[21] and [22].

1.4 Challenges of wind power generation

There are difficulties in estimating the exact wind speed in pre-built urban areas, for instance, capturing the effect of other buildings around the specified location of interest, the reduction in the wind speed caused by the other obstacles and buildings recirculation. Therefore, it is also important that every building around the specific location, has a particular roughness that could affect the wind behavior around the installation location. In other words, to select a suitable building to locate the wind turbine has various challenges mostly occurred by the adjacent buildings and their effect that they could have on the wind velocity around the selected location [5].

Therefore, an advanced tool like Computational Fluid Dynamics (CFD) is a practical, efficient, and affordable way to directly predict and assess the wind speed in site complex urban environments. Some studies focus on computing the wind turbine wake aerodynamics considering the Navier-Stokes equations and using the Computational Fluid Dynamics [23]. Other, CFD methods are considered as an effective tool for estimating the wind energy above the two perpendicular buildings [24], even in investigating the wind pressure coefficient for naturally ventilated buildings, CFD seems to be a reliable tool [25]. CFD is a useful tool to analyze and compare the energy extracted from the wind. In free stream modeling considering the variable metrological characteristics [26].

It is particularly important to choose the correct location of potential turbine mounting locations, especially when it comes to urban areas, as the density of the buildings around the location, could add to the complexity of the wind flow around the selected location of the wind turbine. Uchida used a wind speed design technique in order to evaluate the installation point of a wind turbine using a mesoscale meteorological model and CFD tool [27]. Nedjari evaluated the wake of wind turbines and the soil effects on the wake evolution using a CFD model in complex topography [28].

CFD simulations of the wind flow around a simple building have been conducted in order to assess the effect of different wind conditions on the wind turbines [29], Allard also analyze the wake of a Darrius wind turbine on the roof top of the building using CFD tool (STAR CCM+)[30]. Further

studies indicated that CFD simulations mainly rely on Reynolds Averaged Navier Stokes (RANS) approach, and this approach is known as the most common model used for urban wind applications while Large Eddy simulation is less popular due to its high computational cost [31].

1.5 Objectives and thesis outline

As it has been mentioned before, since the wind speed measurements at specific building locations could be expensive and time consuming, several methods with different degrees of accuracy are available to do an initial assessment of the wind velocity magnitude and wind flow characteristics in an urban area. The method proposed here-in is a numerical method which is based on Computational Fluid Dynamics (CFD). To find the best location on top of the building in terms of energy output, CFD solvers compute the wind velocity and the wind flow around buildings.

In the current work, I exploit STAR CCM+ which is a commercial software to study, model and analyze fluid dynamics problems. As elaborated in upcoming chapters, certain control points are selected above the buildings. The points may represent potential turbine mounting locations. Analysis is then conducted to identify the best locations to install a vertical wind turbine on the roof top of nominated specific buildings in urban areas. At each individual point, wind velocities are extracted from simulations which will then be used to calculate the energy output at each point based on meteorological data. For validation purposes, results derived from simulations are also compared with the experimental data extracted from field measurements at specific locations[32].

This thesis provides an assessment of simulating the wind flow in an urban area. The methodology is applied to two specific test cases on two nominated buildings, one located in King Street and the other one on Guy Street, both in downtown Montréal, Québec using the winter wind rose meteorological data. In this study, we investigate multiple locations in terms of studying the annual total energy output potential, rather than the limited locations that can be studied in experimental methods. The main contribution of this method is that we are using a powerful tool which can study multiple locations at once and have the results within a month which is much faster and more

convenient in comparison with experimental methods e.g., field measurements data, wind tunnels, etc.

Chapter 2 presents the methodology, the turbulence modeling, the inlet velocity profile, boundary condition and meshing. Chapter 3 further explains the test case of the building of interest located on King Street. This chapter also identifies 4 control points above the building to conduct analysis on and presents the calculations of the energy output on the best location above the rooftop of the building. In Chapter 4, the second test case of Concordia EV building on Guy Street is introduced, 4 control points are selected where one is the same location of a study conducted in a wind tunnel on EV building [32]. Calculation and analysis are carried out accordingly and the total energy outputs are verified against the experimental test results. Finally, Chapter 5 provides the conclusion and summarizes deliverables. Research opportunities are proposed to extend or improve the applications of this study in the future work section.

CHAPTER 2: Methodology

2.1 City model

In this study, we use a CAD geometry file which covers a section of the city including a portion of the buildings around the King Street with the building of interest at the center of this geometry. The height of the tallest building in this simulation considered is h, and the dimensions of the computational domain will be constructed based on this length. As the size of the computational domain should not affect the development of the boundary layers, it is crucial to select proper scales around the city so that in the simulation, the boundaries of the computational domain do not have any effects on calculation of the wind flow. The geometrical model of the computational domain has been selected as an octagon because we need to study the wind flow from all 8 principal directions: North, North-west, West, South-west, South, South-east, East, North-east (Figure 3 and Figure 4). The height of the computational domain has been selected as 10 h and the distance between the edge of the city to each boundary is 10 h. Our simulation was based on the recommendations in "*CFD simulations of wind distribution in an urban community with a full-scale geometrical model*"[33].
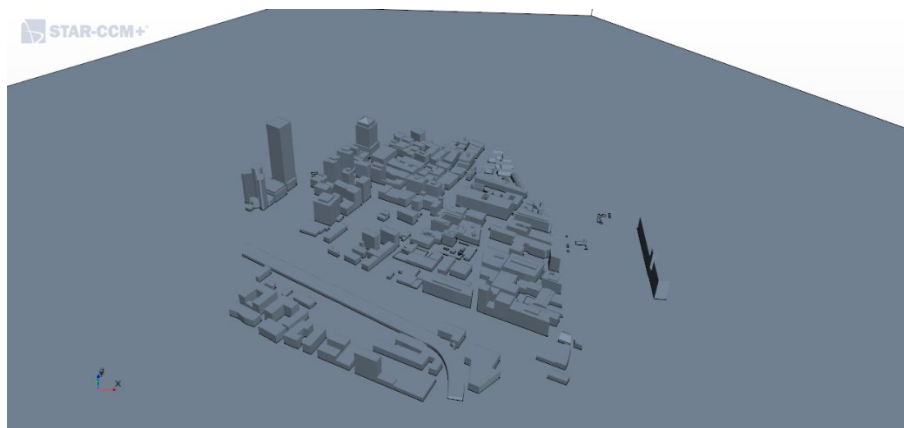
Figure 3: The CAD geometry of test case King Street

Most of the flow founded in the nature is turbulent, especially in engineering applications, hence, the turbulence flow modeling is a principal part of the CFD methodology. The turbulent model is

well described in Hinze[34] "an irregular condition of flow in which the various quantities show a random variation with time and space coordinates, so that statistically distinct average values can be discerned". The presence of eddies of varying sizes in the flow, as well as their diverse interactions, causes these random variations. One of the approached to model turbulence flow is using the Reynolds-Averaged Navier-Stokes (RANS) equations.

2.2 Mathematical Model

2.2.1 Reynolds-Averaged-Navier-Stokes

For turbulent flows, the quantities of the flow such as velocity or pressure of the flow vary dramatically in time and length scale. RANS equation describes the time averaged equation of motion of the flow. In other words, for each quantity, it considers a mean value and the fluctuation to find the exact amount of the quantity

. For instance, for velocity components we can have:

$$u_i = \bar{u}_i + u_i' \tag{1}$$

The amount of these fluctuations could be positive or negative. In STAR CCM+ The averaging process may be thought of as time-averaging for steady-state situations and ensemble averaging for repeatable transient situations [35]. Inserting the decomposed solution variables into the Navier-Stokes equations results in equations for the mean quantities.

The mean mass and momentum transport equations can be written as:

$$\frac{\partial \rho}{\partial t} + \nabla.(\rho\bar{v}) = 0 \tag{2}$$

$$\frac{\partial}{\partial t}(\rho\bar{v}) + \nabla.(\rho\bar{v}\otimes\bar{v}) = -\nabla.\bar{p}I + \nabla.(T + T_1) + f_b \tag{3}$$

Where ρ is the density.

$\bar{v}$ and $\bar{p}$ are the mean velocity and pressure, respectively.

I is the identity tensor.

T is the viscous stress tensor.

f_b is the resultant of the body forces (such as gravity and centrifugal forces).

2.2.2 K-ε turbulence Model

The K-ε Model is based on two exact equations for the Kinetic Energy K, and the dissipation Rate ε. As the Standard model shows an acceptable performance in accuracy and efficiency in modeling a wind field around the building [36], this study attends to simulate the wind flow with Standard k-ε model and Realizable K-ε model[33] in order to decide the optimize model with the best accuracy in simulating the wind flow around the buildings in urban areas. The transport equations for the dissipation rate ε and the turbulence kinetic energy K are:

$$\frac{\partial(\rho k)}{\partial t} + \frac{\partial(\rho k u_i)}{\partial x_i} = \frac{\partial}{\partial x_j}\left[(v + \frac{v_t}{\sigma_k})\frac{\partial k}{\partial x_j}\right] + G - \varepsilon \qquad (4)$$

$$\frac{\partial(\rho\varepsilon)}{\partial t} + \frac{\partial(\rho\varepsilon u_i)}{\partial x_j} \tag{5}$$

$$= \frac{\partial}{\partial x_j}\left[(v + \frac{v_t}{\sigma_\varepsilon})\frac{\partial\varepsilon}{\partial x_j}\right] + C_{\varepsilon1}\frac{\varepsilon}{k}G - C_{\varepsilon2}\frac{\varepsilon^2}{k}$$

$$- C_\mu\eta^3 \frac{1 - \eta/\eta_0}{1 + \beta\eta^3}\frac{\varepsilon^2}{k}$$

where ρ is air density (kg/m3), t time (s), ui and uj the Reynolds time-averaged velocity component in the xi and xj (i, j = 1, 2, 3) directions, respectively, v the dynamic viscosity of air (m2/s), $v_t = C_\mu \frac{K^2}{\varepsilon}$ the turbulence kinematic viscosity (m2/s), σ_k= 0.7194 the turbulence effective Prandtl number for k, G the source term, σ_ε =0.7194 the turbulence effective Prandtl number for ε,

$C_{\varepsilon1} = 1.42$

$C_{\varepsilon2} = 1.68$

$C_\mu = 0.085$

$\eta = (2E_{ij}.E_{ij})^{\frac{1}{2}}\frac{k}{\varepsilon}$

$E_{ij} = \frac{1}{2}(\frac{\partial u_i}{\partial x_j} + \frac{\partial u_j}{\partial x_i})$

$\beta = 0.012$

$\eta_0 = 4.38$

In the settings of STAR CCM+ for the turbulence models, we have two choices to select, first we select the Realizable K-ε model and other physical models as it has been demonstrated in [37]. In the second phase of this study, we will run the same simulation using the Standard k-ε model to find the more accurate turbulence model to simulate the wind flow field over the buildings in an urban area.

The turbulent eddy viscosity μ_t is calculated as:

$$\mu_t = \rho C_\mu f_\mu KT \tag{6}$$

where:

ρ is the density.

C_μ is a Model Coefficient.

f_μ is a Damping Function.

T is the turbulent time scale.

In STAR CCM+, the transport equations for the kinetic energy K and the turbulent dissipation rate ε are:

$$\frac{\partial}{\partial t}(\rho k) + \nabla \cdot (\rho k \overline{V}) \tag{7}$$

$$= \nabla \cdot \left[\left(\mu + \frac{\mu_t}{\sigma_k} \right) \nabla k \right] + P_k - \rho(\varepsilon - \varepsilon_0) + S_k$$

$$\frac{\partial}{\partial t}(\rho \varepsilon) + \nabla \cdot (\rho \varepsilon \overline{V}) \tag{8}$$

$$= \nabla \cdot \left[\left(\mu + \frac{\mu_t}{\sigma_\varepsilon} \right) \nabla \varepsilon \right] + \frac{1}{T_e} C_{\varepsilon 1} P_\varepsilon$$

$$- C_{\varepsilon 2} f_2 \rho \left(\frac{\varepsilon}{T_e} - \frac{\varepsilon_0}{T_0} \right) + S_\varepsilon$$

where:

$\overline{V}$ is the mean velocity.

μ is the dynamic viscosity.

σ_k , σ_ε , $C_{\varepsilon 1}$, and $C_{\varepsilon 2}$ are Model Coefficients.

P_k and P_ε are Production Terms.

f_2 is a Damping Function.

S_k and S_ε are the user-specified source terms.

ε_0 is the ambient turbulence value in the source terms that counteracts turbulence decay. The possibility to impose an ambient source term also leads to the definition of a specific timescale T_0 that is defined as:

$$T_0 = \max(\frac{k_0}{\varepsilon_0}, C_t \sqrt{\frac{\nu}{\varepsilon_0}}) \tag{9}$$

2.2.3 K-epsilon Standard Model
The Standard K-Epsilon model is a *de facto* standard version of the two-equation model including transport equations for the turbulent kinetic energy k and its dissipation rate ε. The transport equations are of the form suggested by Jones and Launder [38], with coefficients suggested by Launder and Sharma [39]. In STAR-CCM+, certain new terms have been introduced to the model to account for phenomena like buoyancy and compressibility. A non-linear constitutive relation is also available as an option.

2.2.4 K-epsilon Realizable Model

The Realizable K-Epsilon model contains a new transport equation for the turbulent dissipation rate ε [40].In addition, rather than being assumed to be constant as in the conventional model, a critical coefficient of the model C_μ is stated as a function of mean flow and turbulence properties. This approach allows the model to satisfy specific mathematical limitations on normal stresses that are consistent with turbulence science (realizability). The concept of a variable C_μ is also supported by experimental findings on boundary layers.

For many situations, this model outperforms the Standard K-Epsilon model and may be depended on to provide results that are at least as accurate. In STAR-CCM+, both the standard and realizable models can be utilized with fine meshes that resolve the viscous sublayer, thanks to the possibility of utilizing a two-layer method.

2.3 Test Case Description

In this study the potential energy output and wind velocity above a building in King Street is investigated. 4 control points have been set at the 4 corners of the roof top of the building at 5 m. These same points were also considered for potential turbine mounting locations of a 2 m height Troposkien turbine with NACA 0012 airfoil section and three blades is a previous work [41]. In this case, the inlets and outlets for the octagonal computational domain is fixed and the results are assessed with observing the flow behavior above the roof top. For this observation, the streamlines and the velocity vectors above the roof top are used to study the wind velocity above the building and compare the velocity magnitude at 4 control points. We expect to have the highest velocity at location 3 which represents the west side of the building as the most wind is from west in Montreal regarding the meteorological data. Figure 4 provides the isometric view of the dimensions of the octagonal computational domain. The height of the computational domain is 10 h (h is the height of the highest building in the considered area) and the distance between the edge of the city area to the boundary of the octagon is 10 h in each direction [33].
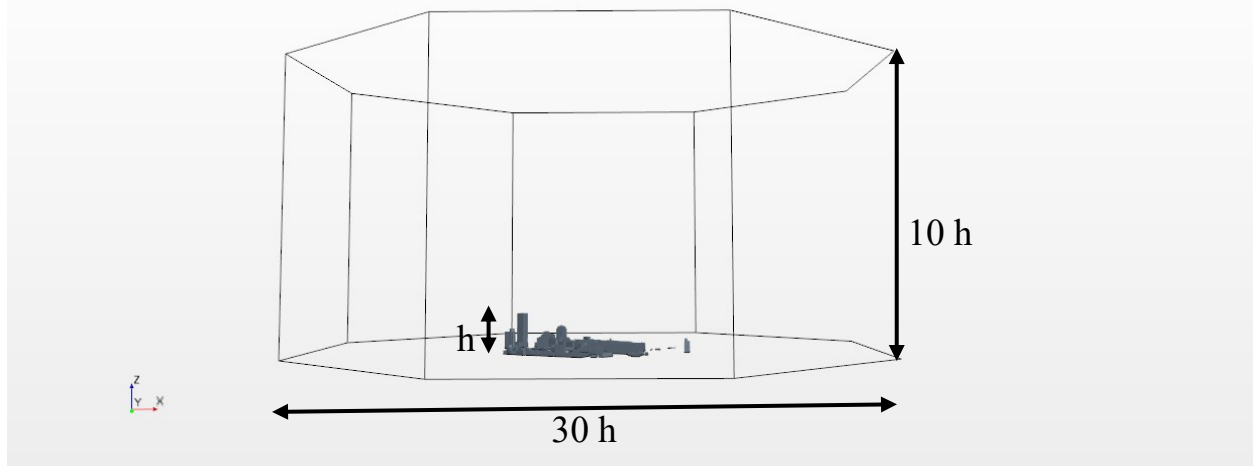
Figure 4: The isometric view of the dimensions of the computational domain

2.4 Boundary Conditions

In this case, 8 different scenarios have been designed to assess the wind direction impact on wind behavior around the building and eventually the energy output in 4 locations above the EV building. In each scenario, one specific wind direction is simulated, and 3 adjacent faces exposed by that specific wind direction (Figure 5) are considered as the inlet velocity (Figure 6), and the corresponding 3 faces in front were selected as the outlet, and the other faces were set accordingly. For instance, if the wind direction is from the west, the velocity inlet is set for faces north-west, west and south-west (Figure 7). The top, north and south faces are then defined as no slip boundary condition and the east, north-east and south-east are selected as pressure outlet with the gage pressure of 0. The turbulent intensity of 0.1 is set as the initial condition and turbulent viscosity ratio is kept as the default value of 10 [42]. The turbulent intensity is defined as the ratio of the root-mean-square of the velocity fluctuations, to the mean flow velocity.
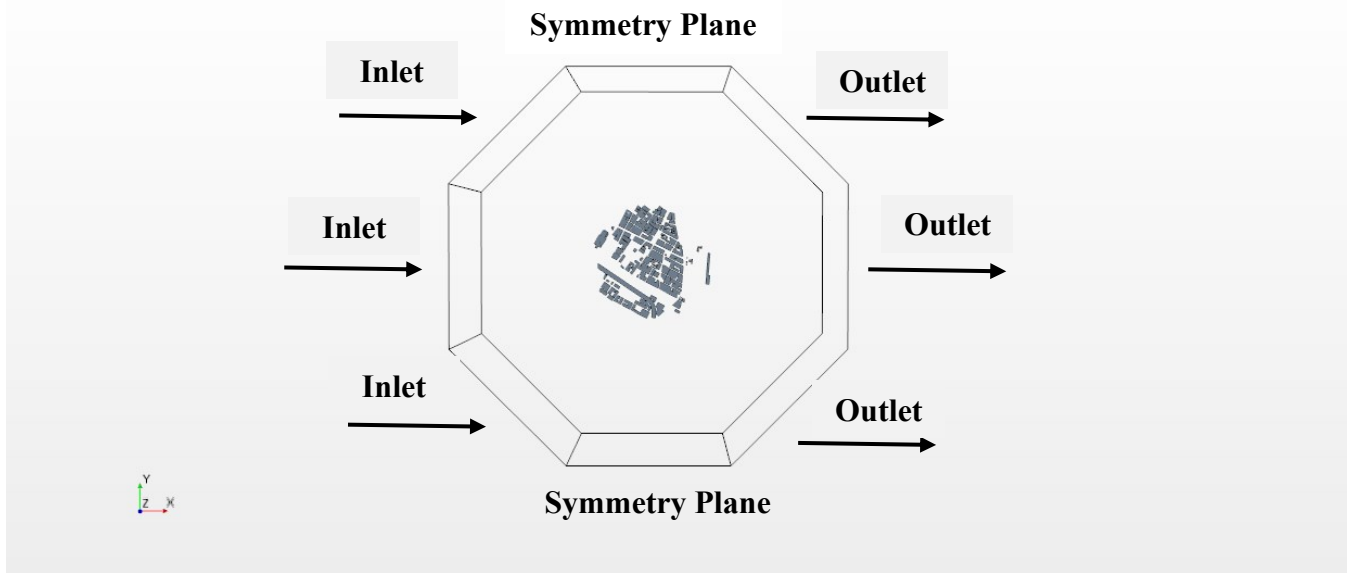
Figure 5: The isometric view of the boundary condition of each side of the octagonal computational domain
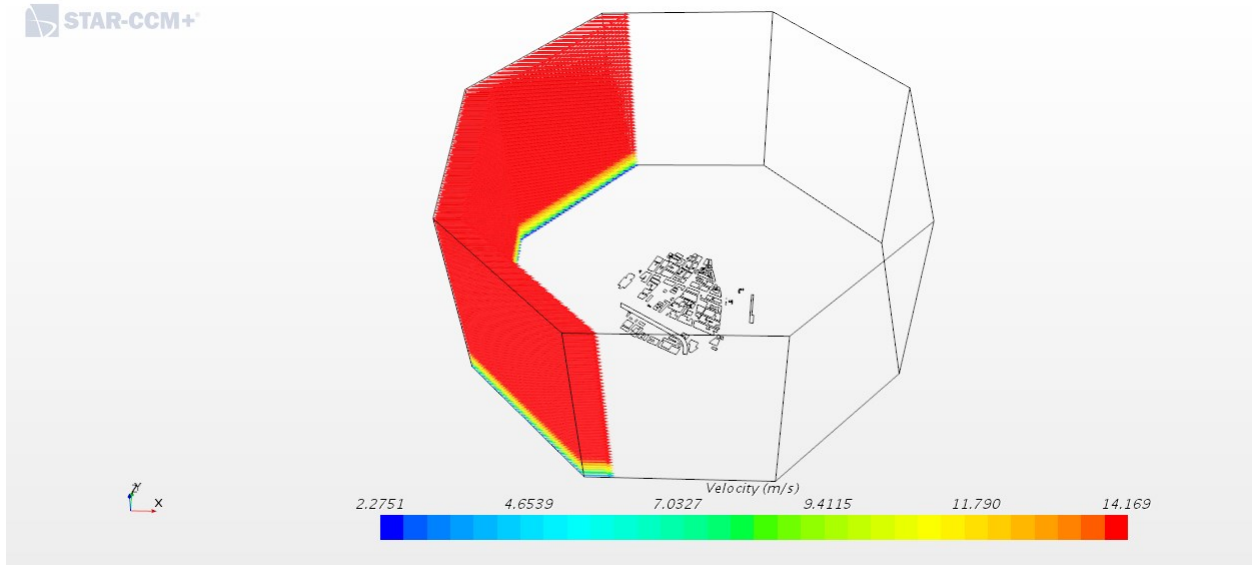
Figure 6: The velocity inlet profile on three adjacent faces exposed to the wind direction
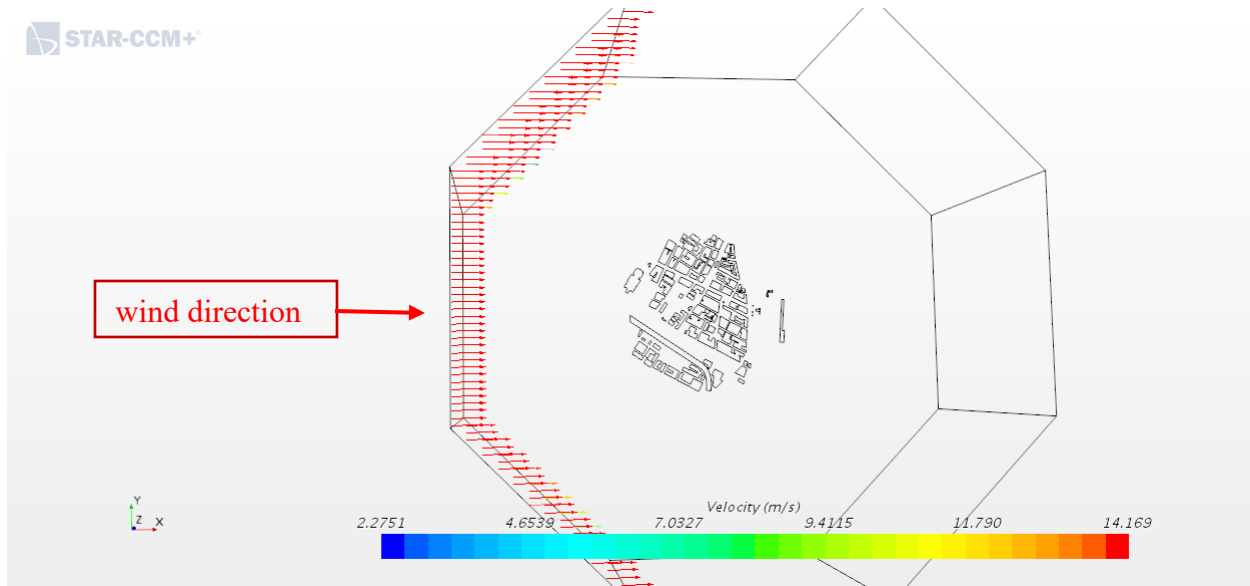
Figure 7: Three adjacent faces which are exposed to the wind direction are selected as inlet velocity.

2.4.1 Velocity Inlet Boundary Condition

For setting the velocity of the inlet flow, we have three options: velocity inlet, mass flow inlet and pressure inlet. In this study, we set the velocity of the wind flow at the inlet of the computational domain, so that we must use the velocity inlet.

2.4.2 Inlet Velocity Profile

The implementation of wind velocity profile must include the effect of atmospheric boundary layer. To take the wind velocity profile as the inlet velocity profile of the computational domain, we need to consider the velocity as a function of the height, as the equation below:

$$V_z = V_{top} * (\frac{Z}{H_t})^{0.31} \tag{10}$$

Where V_{top} is the velocity at the reference height (m/s), Z is the height from the ground (m), H_t is the height from the ground to the reference point(m) and V_z is the mean velocity profile(m/s). We

17

have the height of our computational domain as the Z, by applying the coordinates of our computational domain, we can calculate the wind flow velocity and set it as the inlet velocity (Figure 8 and Figure 9).
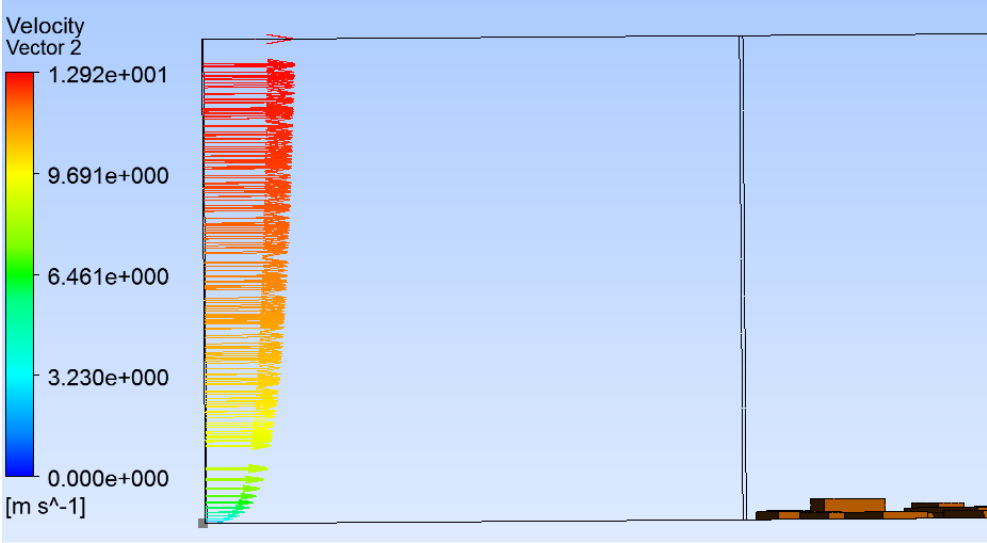
Figure 8: The wind velocity profile that has been set at the inlet as inlet velocity.
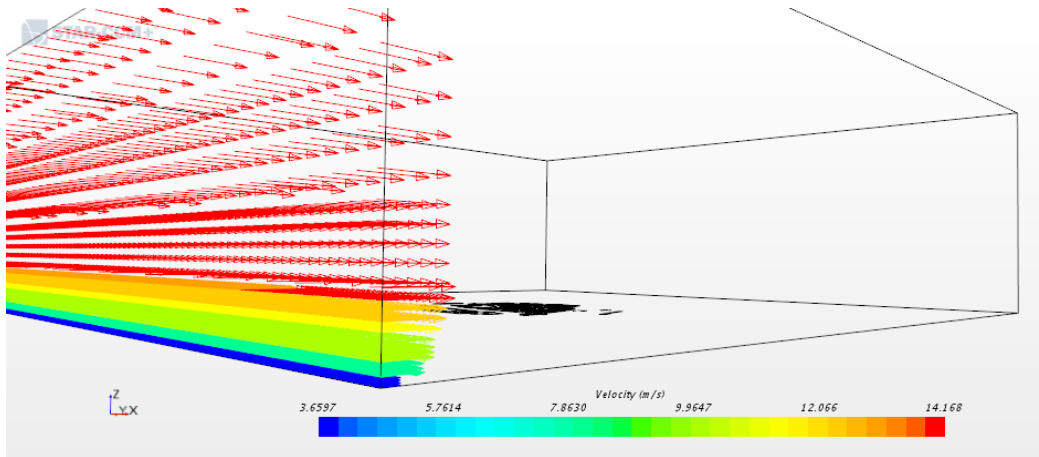
Figure 9: The wind profile which has been set as the inlet velocity in STAR CCM+

2.4.3 Pressure outlet Boundary Condition

STAR CCM+ offers different options for the outlet of the domain, such as outflow boundary condition, pressure far-field and pressure outlet. In some cases, when we might have the backflow, we should use the option outflow because we have no information about the velocity or the pressure on the outlet prior to the solution of the problem. In this case, since we consider the outlet far enough from the building, we can choose the Pressure outlet boundary condition, as is used for all the cases of validation and roof mounted wind turbine analysis [43].

2.4.4 Symmetry Plane Boundary Condition

The symmetry plane boundary condition can be used while the flow's behavior is expected to be symmetrical about the plane that divided the domain into two symmetrical parts. we can use the symmetry boundary condition when the expected pattern of the flow is mirror symmetry, we also could use the wall boundary with zero shear slip wall in viscous flow. The top plane and 2 adjacent faces of the octagonal contiguous to the inlet and outlet were set to Symmetry Plane boundary condition.

2.5 Mesh Setup

In this study, as the buildings in the computational domain have simple geometrical shapes, we can choose between the tetrahedral cells (Figure 10) or the trimmed cells (Figure 11). To investigate the grid sensitivity, the same mesh size has been used for both mesh models. Although

19

the tetrahedral model creates much larger number of cells and cause an expensive simulation, it provides more precise and high-quality cells above the building. As an example, for creating 5 cm cells above the building, with the tetrahedral method the amount of the total cells is 25 million while with trimmed mesh, the mesh size was 9 million. Hence, the tetrahedral model has been selected for discretizing the computational volume into volumetric elements that are used in the computations and the trimmed model used to mesh the prism layers (inflation layers) around the selected building.

 In this simulation, we start with 5 million cells, fine inflation layers with trimmed cells are created around all buildings and near the walls and the ground to capture the flow details better. Moreover, to study the mesh independence, we have refined the mesh to 10 million and 20 million. The objective is to reach the mesh independent results and to identify the optimize mesh size.
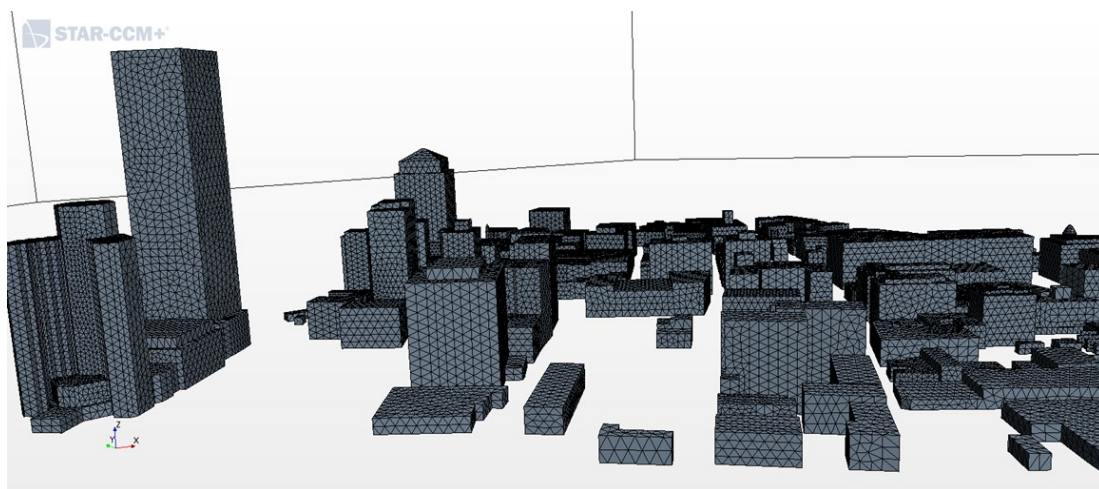
Figure 10: The tetrahedral mesh over the buildings around the King Street
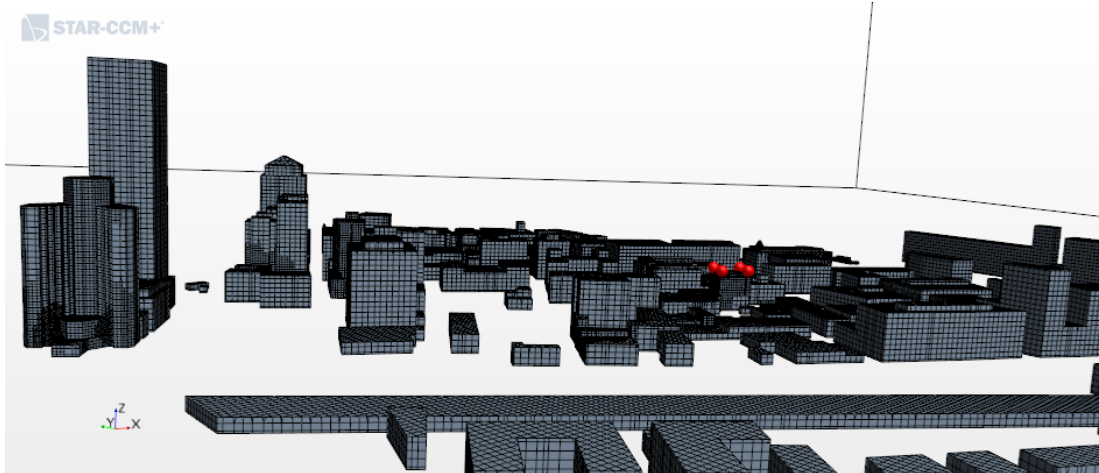
Figure 11: The Trimmed mesh over the buildings around the King Street

Figure 12 demonstrates the 3D view of the tetrahedral mesh of the whole building zone, the total mesh size is 10 million with using prism layers and finer mesh cells around the buildings and near the ground. The mesh around the buildings has 10 prism layers to improve the assessment of the flow near to the surface of the building Figure 13.
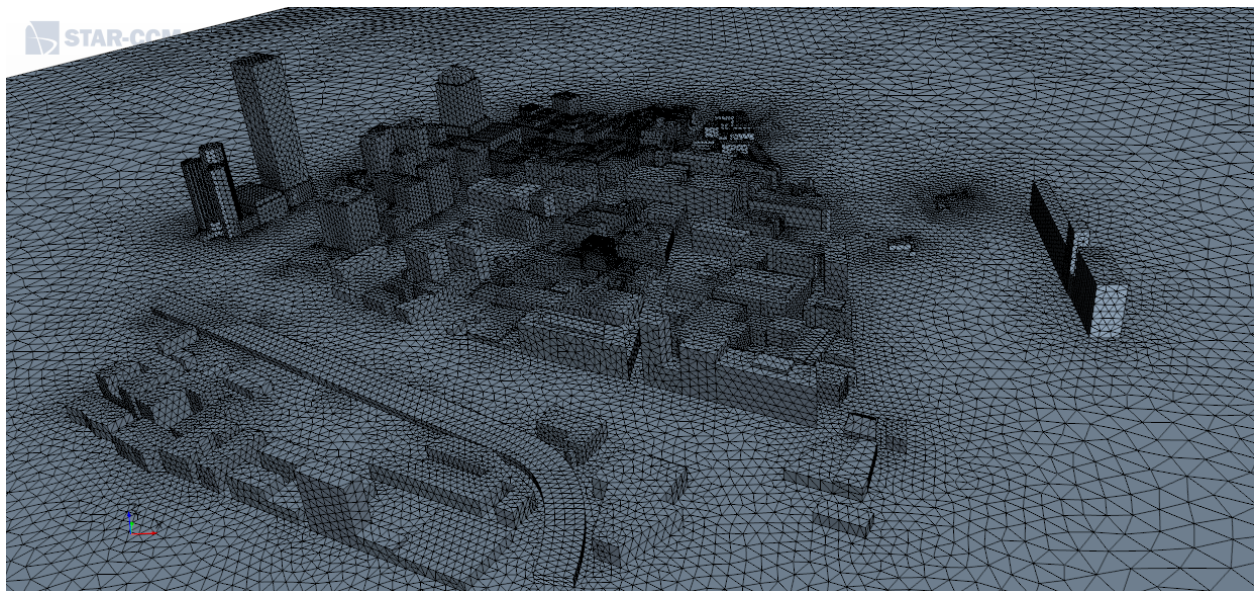
Figure 12: The tetrahedral mesh with 10 million cells in building zone
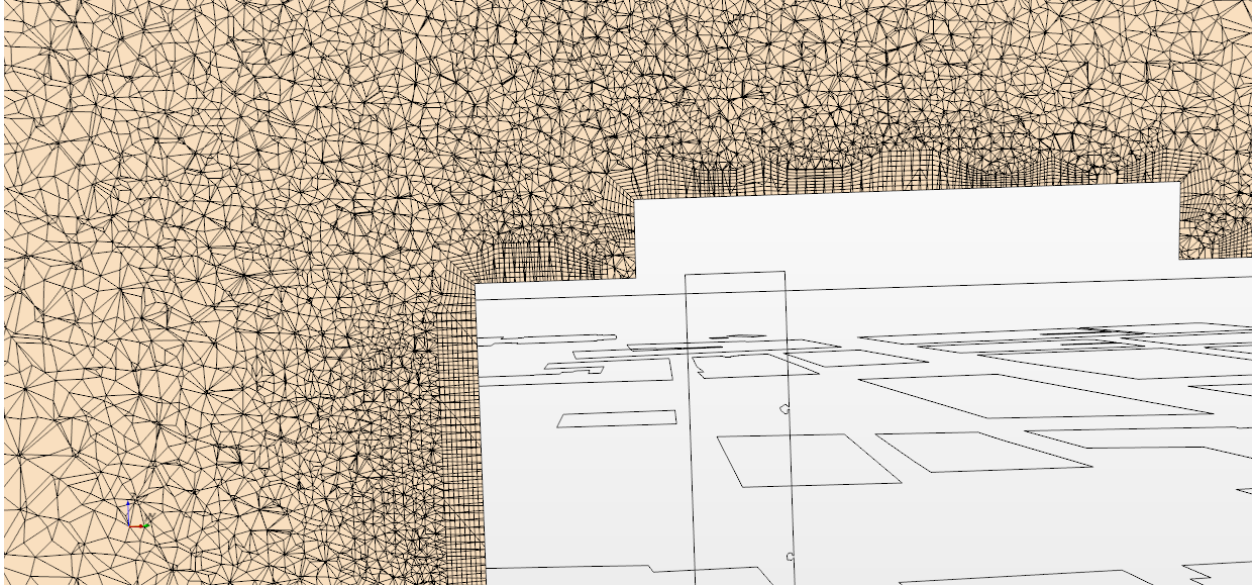
Figure 13: The mesh cells above the building with minimum amount of 0.09 and maximum amount of 0.2 meter (on the surface of the root top)

The value of y+ above the building are calculated by the software and are plotted in Figure 14. The size of the first cell in the mesh methodology has been selected so that the amount of y+ above the building is more than 10 and less than 100 (in k-epsilon models the preferable value for y+ is between 30 to 300 [44]). Figure 14 shows the isometric view of the y+ on the buildings, the finer mesh around the selected building in King Street results to much less amount of y+ round of this building (around 58 mostly) in comparison with other buildings.
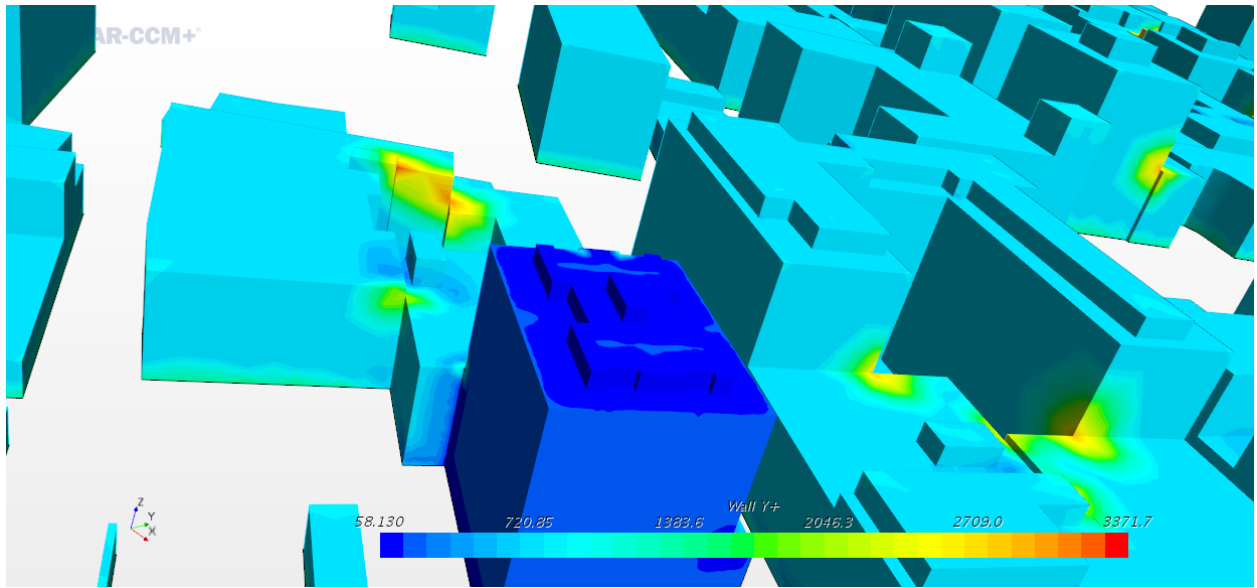
Figure 14: Wall Y+ around and at the roof of the building

CHAPTER 3: Model Verification

3.1 Mesh Verification

Since the solution is affected by the mesh size, the objective of this section is to find the mesh independent solution so that the results would be valid. The grid sensitivity is investigated by using three different mesh sizes to study the effect of mesh size on the results and to evaluate the wind speed at the same points with keeping the same parameters in the solver. The mesh size was started by having 5 million cells and then finer the mesh sizes were constructed to have 10 million and 20 million cells in the computational domain.

In this section, we also investigate two turbulence models, first run is based on Realizable K epsilon model, and the second run is based on the Standard K epsilon model. After running these two simulations with the same geometry, mesh, and settings but different turbulence models, we can extract different data sets such as the velocity at 4 control points, the streamlines, the turbulence kinetic energy etc.
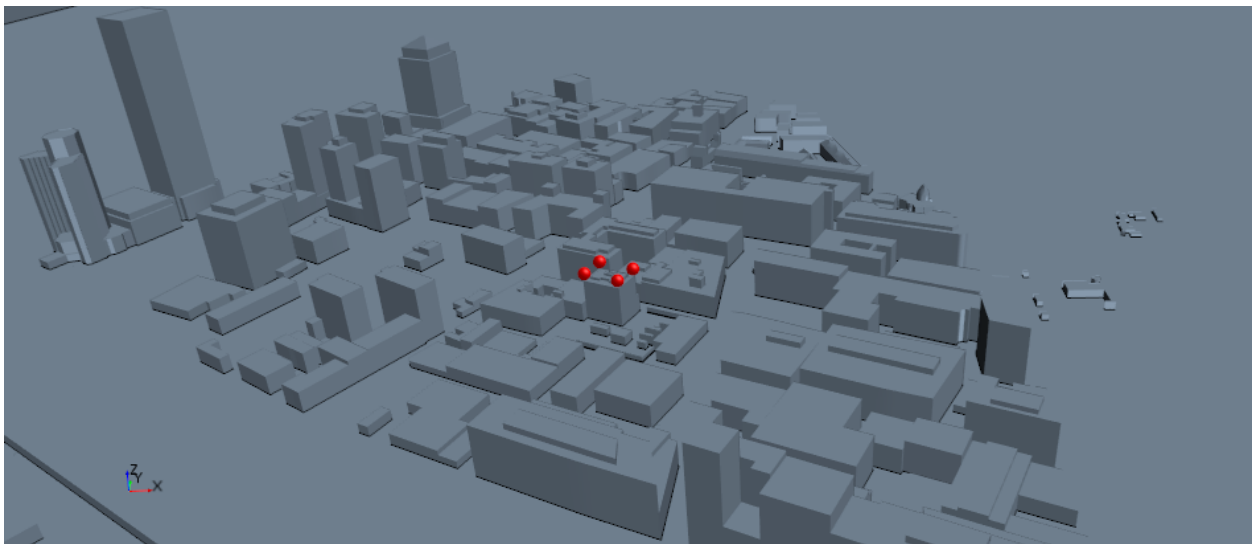
Figure 15:Four control points at the edge of the rooftop represented as 4 possible locations for installation of wind turbines

Also, we will provide a table which includes the velocity at 4 control points in Figure 15 in both simulations. In this table we can compare the velocity difference for the same point. This could be criteria of selecting the optimized turbulence model. We set all these control points at the edge of the rooftop of the selected building, to record the velocity magnitude in that specific location.

Figure 16 shows the building zone meshes and the prism layers around the building to achieve finer cells around the selected building. To investigate the grid sensitivity, we have three meshes with 5, 10 and 20 million cells to have three different densities around the building.
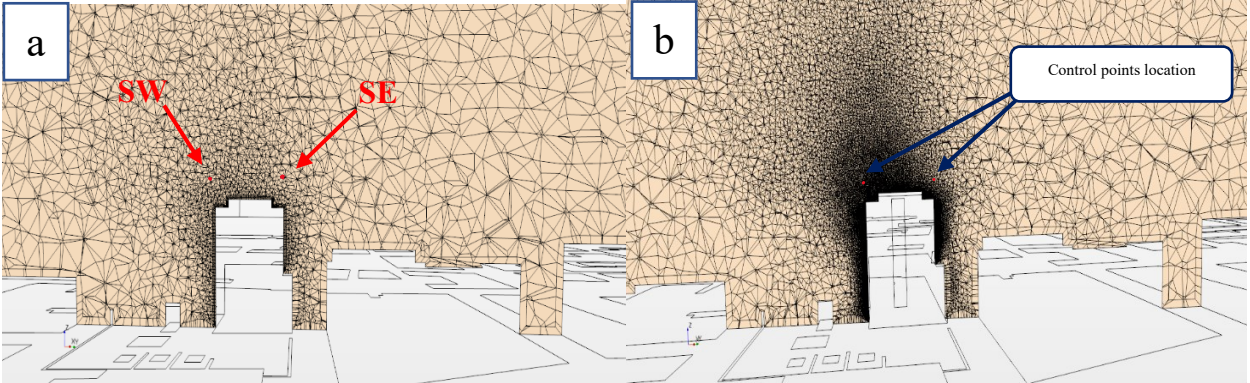
Figure 16: A vertical section of the mesh in a) 10 million mesh with the location of control points of South-West and South-East. b) 20 million mesh above the building to investigate the mesh sensitivity and the location of the control points at South-west and South-east
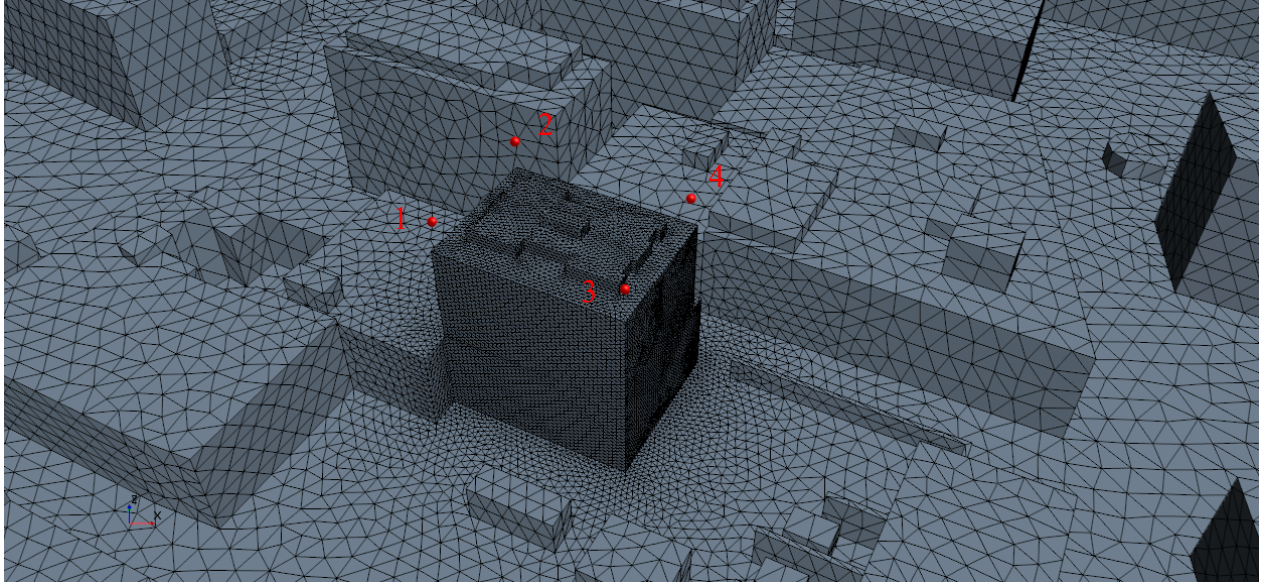
Figure 17: The 3D view of the building indicating the locations of 4 control points above the building roof

In each case, the finer mesh has twice the number of cells with more accumulation around the building. In Table 1, the velocity magnitude at each four points above the building is extracted. In Figure 16, the control points 1 and 2 represent the North-west and North-east respectively, and the control point South-West represents point 3 while the South-east location represents point 4. The mean difference for the finer mesh prediction of velocity magnitude is less than 2%. Figure 17, shows a 3D view of the surface mesh on the building and surrounding buildings. Furthermore, as indicated, the mesh size is gradually growing as moving outward from the building.

Table 1: Velocity magnitude at 4 control points using K-epsilon standard turbulence model while the wind if from South-West direction

Standard	Point 1	Point 2	Point 3	Point 4
5 million	5.96	6.05	5.19	4.04
10 million	6.04	6.15	5.94	4.52
20 million	6.29	6.85	6.02	4.69

Table 2: Velocity magnitude at 4 control points using K-epsilon realizable turbulence model while the wind if from South-West direction

Realizable	Point 1	Point 2	Point 3	Point 4
5 million	7.11	8.23	6.37	4.65
10 million	8.01	8.33	7.06	4.77
20 million	8.36	8.39	7.09	5.03

In both tables the highest velocity magnitude difference occurs at point 2 which is at the south-west side of the building (Figure 18). In Table 1, the lowest difference of wind velocity occurs at point 4, this situation is the same for Table 2. The realizable turbulent model seems to calculate higher amount of velocity magnitude at the roof top of the building in comparison with the data of the standard turbulence model in Table 1. By increasing the mesh size from 5 to 10 million and from 10 to 20 million, the velocity magnitude in realizable model varies in higher rates than in standard model. In Figure 18, The wind rises from the west side of the building, it is shown that the velocity magnitude decreases after it reaches the point 4 at the back of the building at the east side.
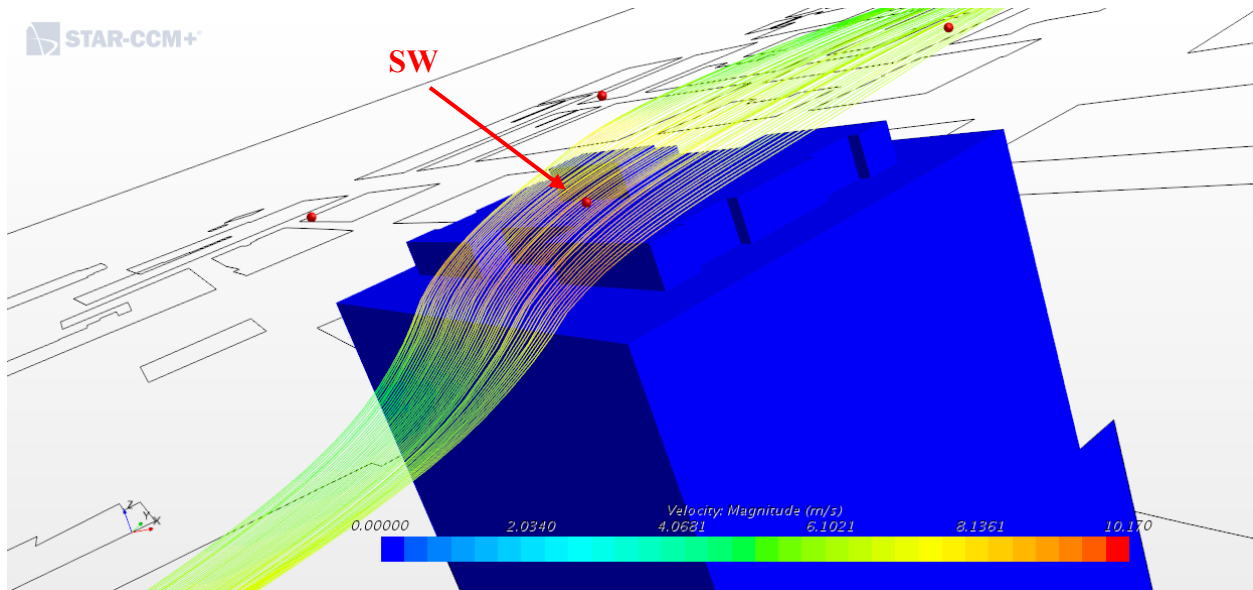
Figure 18: The streamlines of wind velocity above the building

The convergence residuals of both turbulent models are provided in Figure 19 and Figure 20. The results of velocity magnitude at each four points for each turbulence model extracted after 10000 iterations and the amount of the residuals for continuity and kinetic energy and momentums are controlled to reach stable results. The residuals are in the order of e-3 or lower (Table 3) and the plot of the residual vs iterations demonstrates that the residuals seem to reach a stable value through the iterations. To investigate the convergence of the results, the velocity magnitude at a specific point in terms of iteration is plotted.
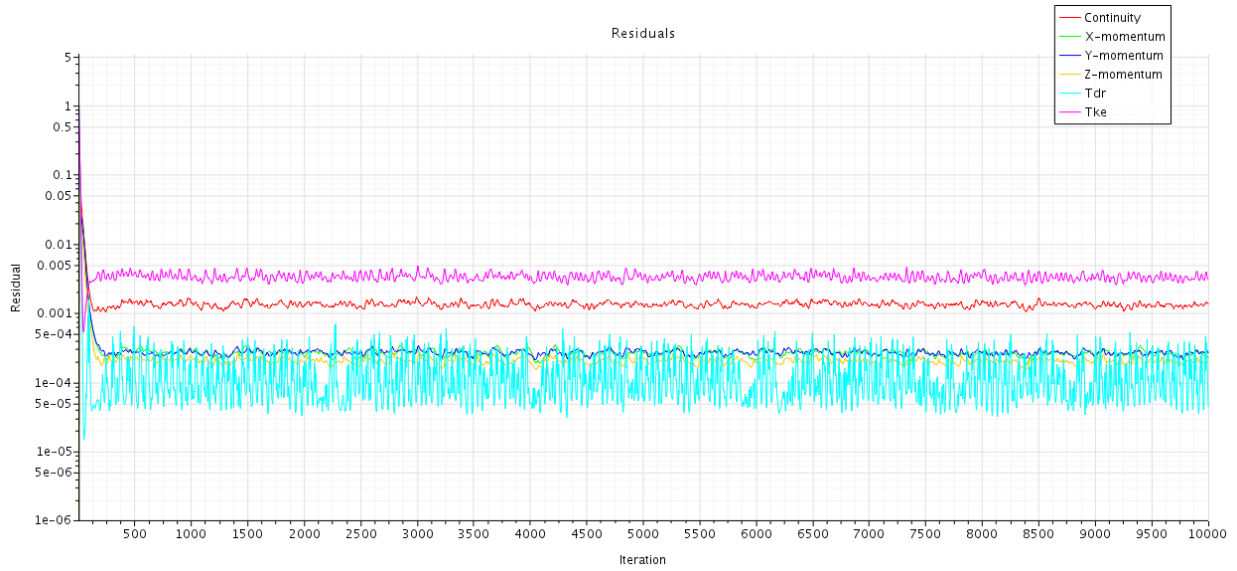
Figure 19: Residuals of the solution using k-epsilon Realizable model
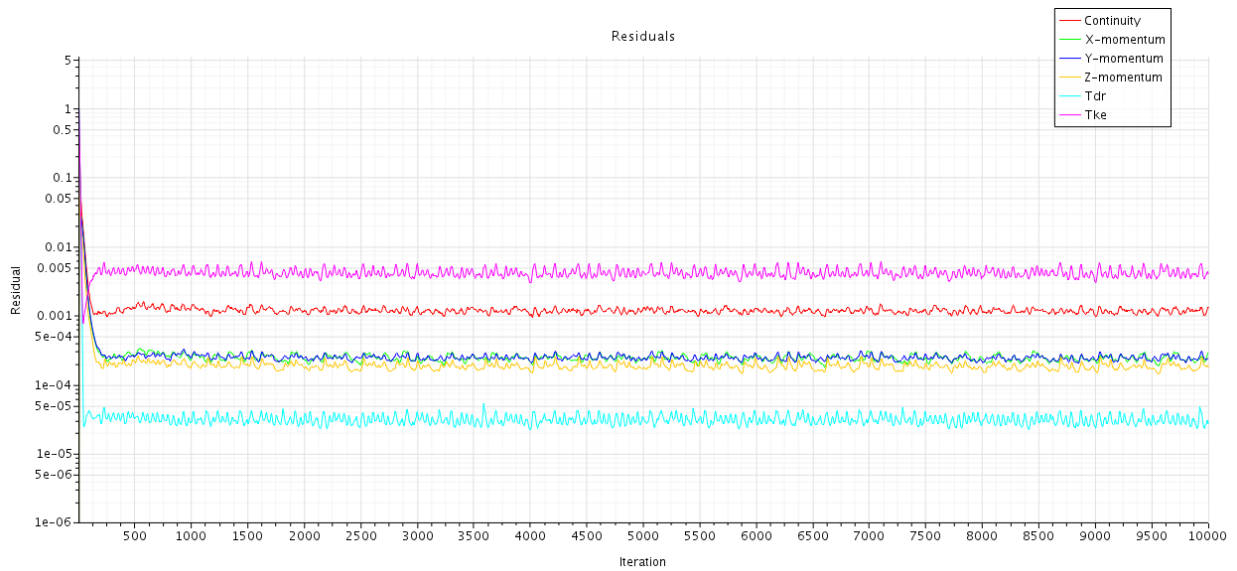
Figure 20: Residuals of the solution using k-epsilon Standard model

The residuals in both models are in the same level of accuracy, and the accuracy of the residuals are almost around e-4.

Table 3: The residuals amount for each model

	Iteration	Continuity	X-momentum	Y-momentum	Z-momentum	TKe	Tdr
Realizable	10000	1.349654e-03	2.219163e-04	2.579751e-04	1.883502e-04	3.076609e-03	4.327229e-05
Standard	10000	1.427646e-03	2.918673e-04	3.295226e-04	2.137027e-04	4.533280e-03	3.117104e-05

3.2 Convergence

The convergence of the results is also investigated by plotting the velocity magnitude versus the iteration number. The difference or fluctuation of the velocity magnitude at each control point for both models should be minimal. Figure 21 shows that the solution has converged, and the results will be in the same range for more iterations. The velocity value after 10000 iterations at point 3 is 6.038 m/s and the velocity magnitude at the same point at iteration 10800 is 6.05 m/s.
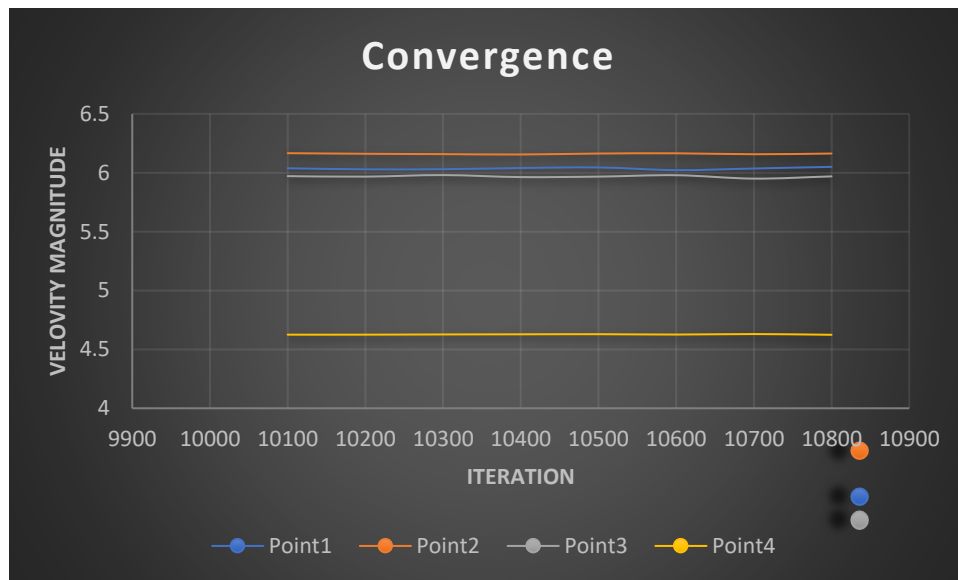
Figure 21: The velocity magnitude changes with 1000 iterations at all control points

3.3 Discussion

In this chapter, the flow behavior around the roof top is evaluated and analyzed for both turbulent models, i.e., Standard k-epsilon and Realizable k-epsilon. For each specific model, the wind flow velocity and the streamlines around the buildings are derived and extracted from the software, accordingly, velocity vectors are shown around the building roof with 10 million mesh cells. The corresponding contours for each turbulent model have been illustrated for Turbulent kinetic Energy and Vorticity around the building in the King Street and the wind direction in the below extracted figures is from West.

3.3.1 Wind Velocity Profile in the Vertical Plane

To investigate the velocity of the flow at the top of the building and around the edges, we investigate a vertical plane which crosses the building at the centerline. The velocity of the wind flow over the whole computational domain reveals the wind behavior around the urban area Figure 22.
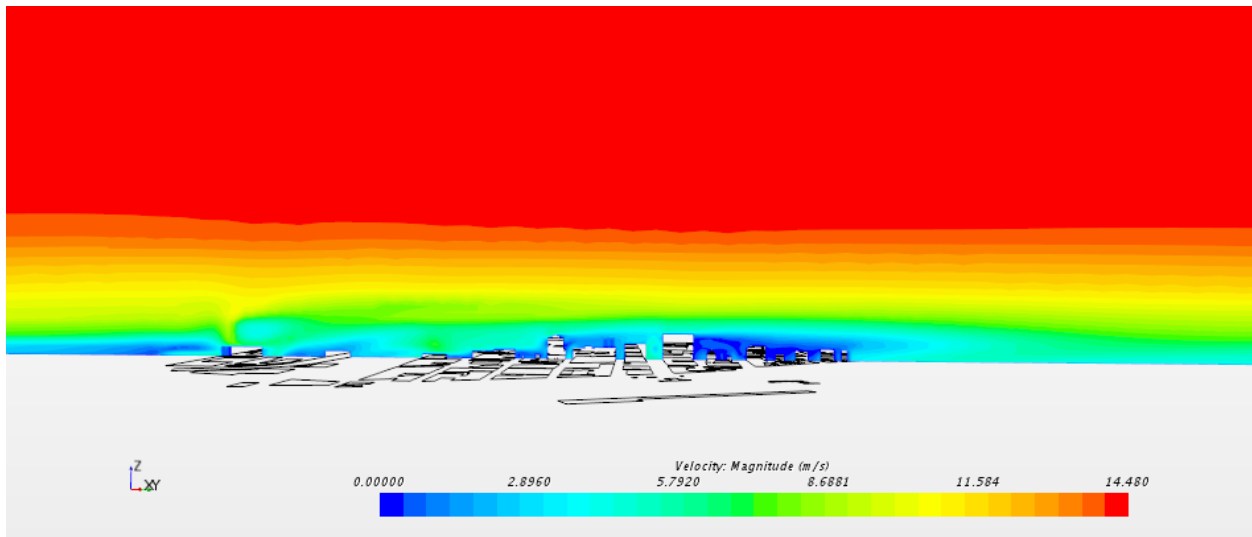
Figure 22: The velocity of the wind flow plotted on the vertical plane goes through the centerline of the building using k-epsilon Realizable model
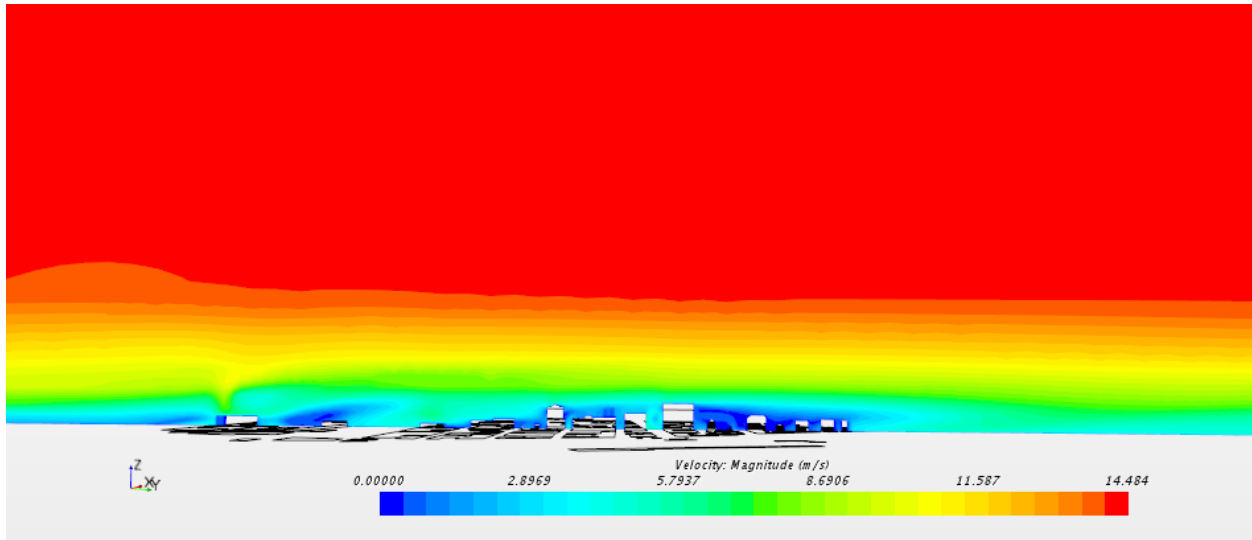
Figure 23: The velocity of the wind flow plotted on the vertical plane goes through the centerline of the building using k-epsilon Standard model

The velocity over the building is illustrated as below in Figure 24, we can see that the velocity of the wind is higher at the front edge of the building compared to the rear edge of the building. This could be an indication to conclude that the best location for the wind turbine could be in the two control points at the front edge of the building. More data could be extracted from the exact velocity magnitude at those two points in the front edge to decide between those two control points.
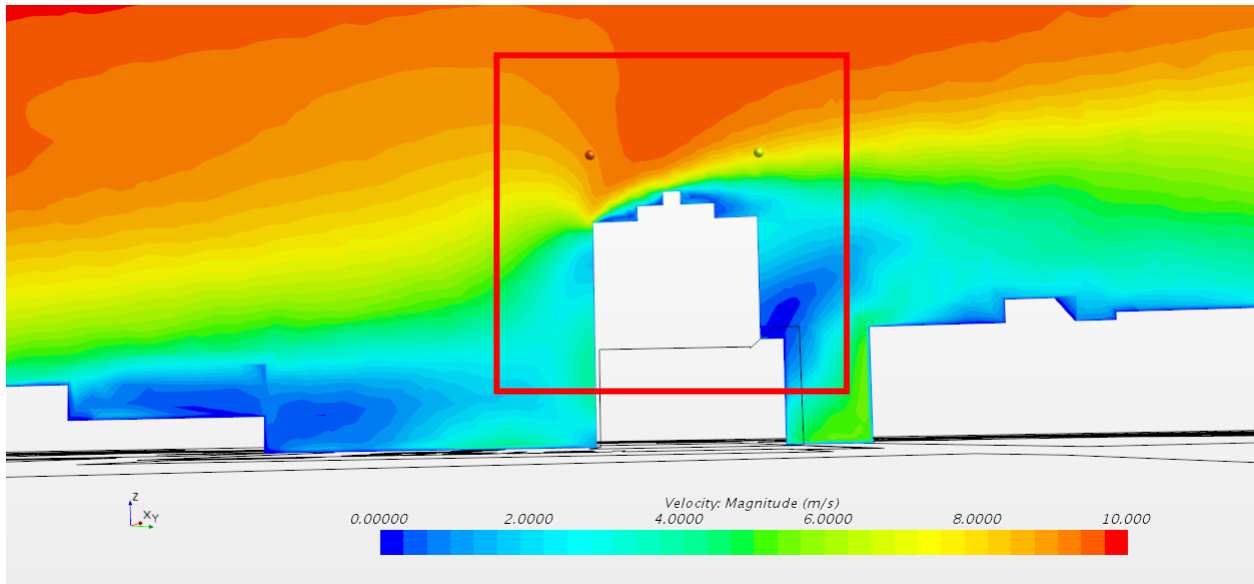
Figure 24: The wind flow field above the building using k-epsilon Standard model
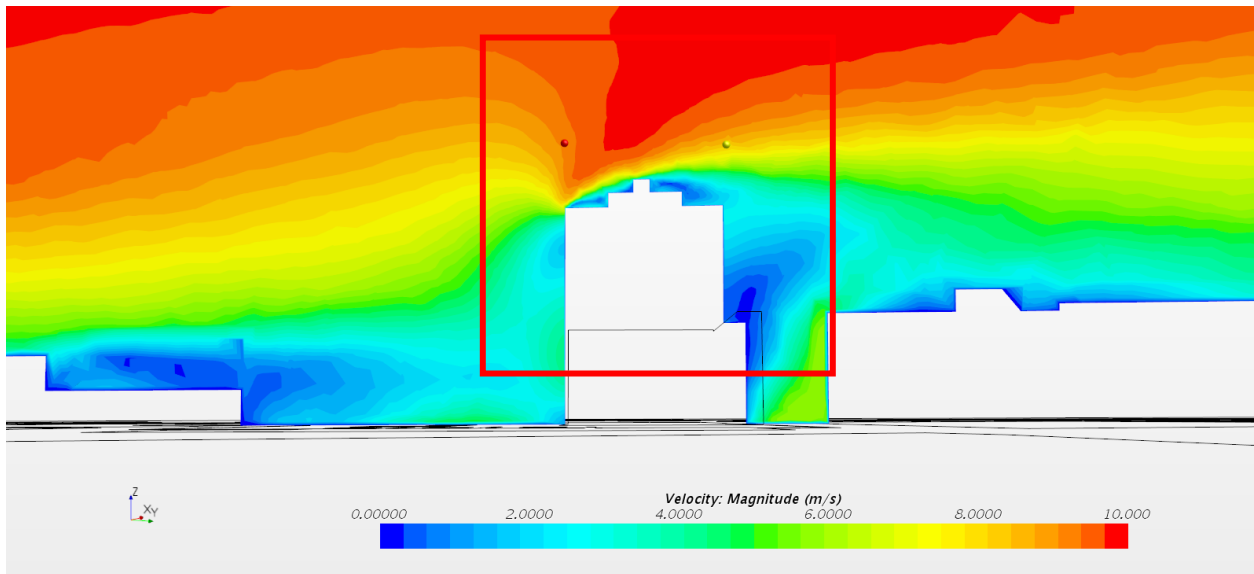
Figure 25: The wind flow field above the building using k-epsilon Realizable model

In both models, the results seem to be fair and the contours around the building and on the rooftop of the building seems to be almost the same as the K-epsilon model. The velocity in the computational domain seems to have higher range in Realizable model compared to the Standard model.

3.3.2 Velocity Vectors on the Vertical Plane Around the Building

The velocity vectors in Figure 27 shows the wind flow direction around the buildings and specifically demonstrate the location of the wakes or vortexes between the buildings. These are the locations which should be avoided to install a wind turbine due to the reduction of the wind velocity.
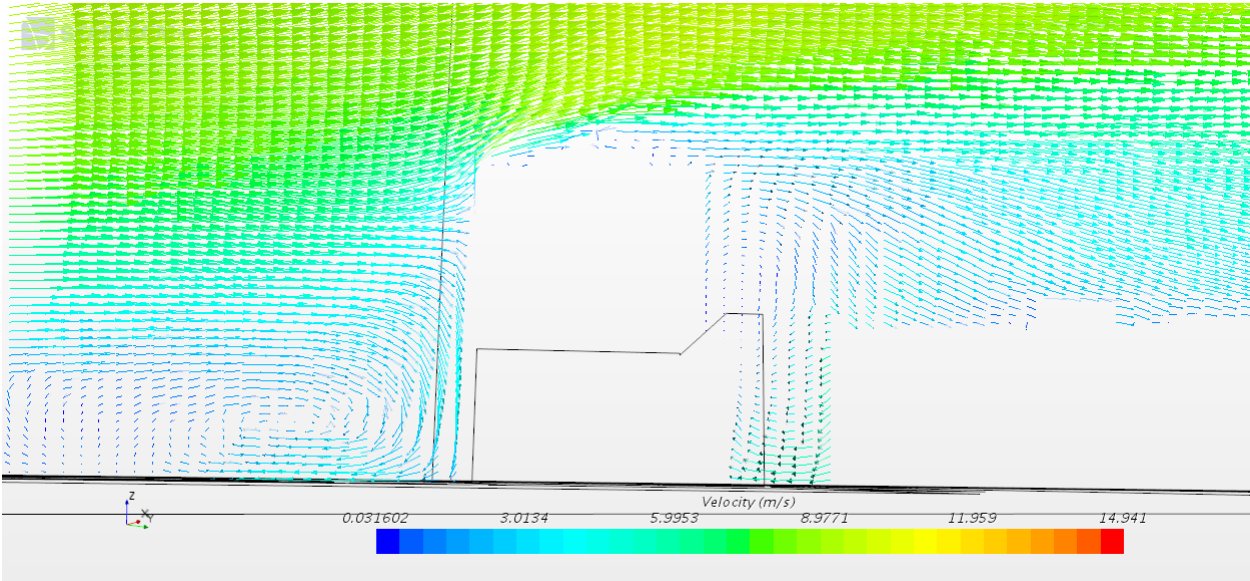
Figure 26: The velocity Vectors around the buildings on the Vertical plane in k-epsilon Standard model
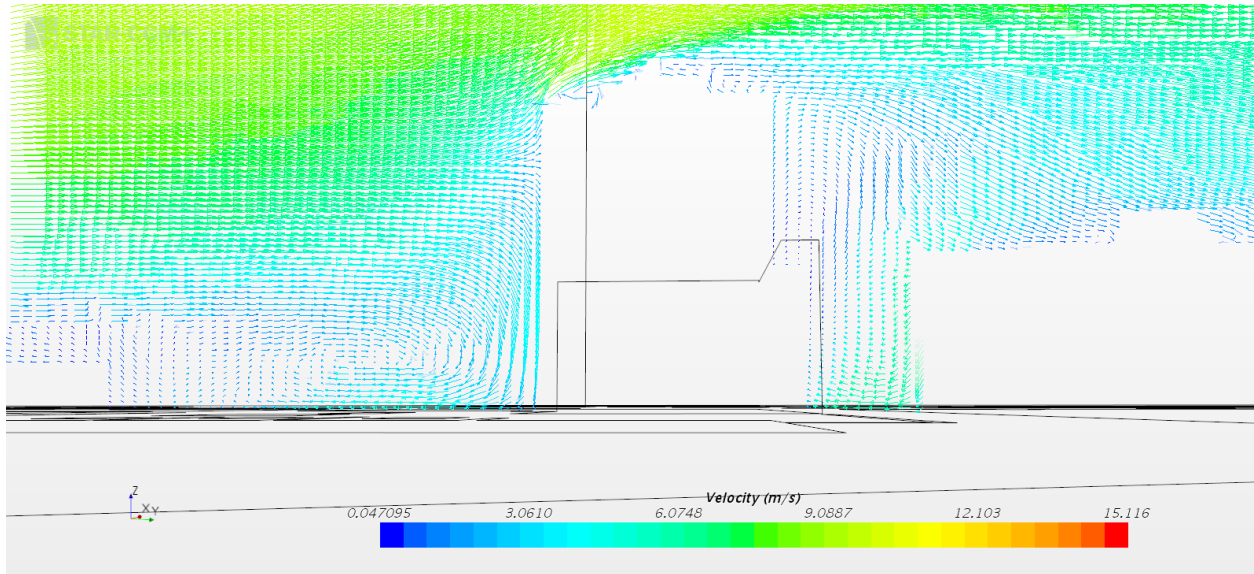
Figure 27: The velocity Vectors around the buildings on the Vertical plane in k-epsilon Realizable model

3.3.3 3D Flow Streamlines in the domain_ A Narrow Set of Streamlines Around the Building
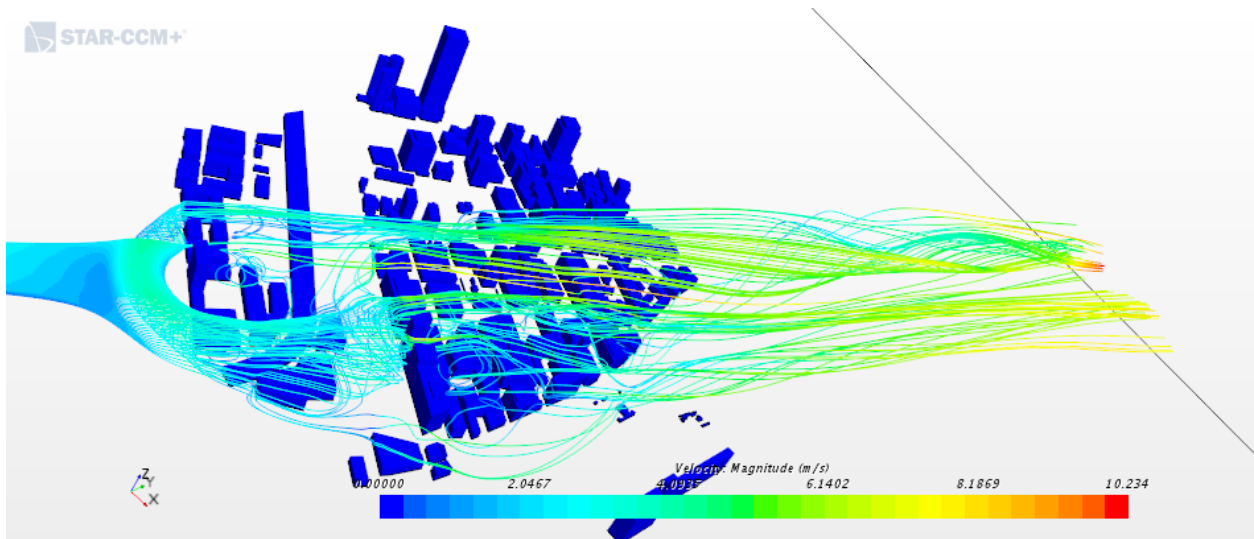
Figure 28: A 3D narrow set of flow streamlines from West direction and the movements of each streamline through the whole computational domain using k-epsilon Realizable model

The streamlines show the general behavior of the wind flow around the building, in Figure 29, the wind flow move above the building and with higher velocity at the front edge compared to the rear edge of the building.
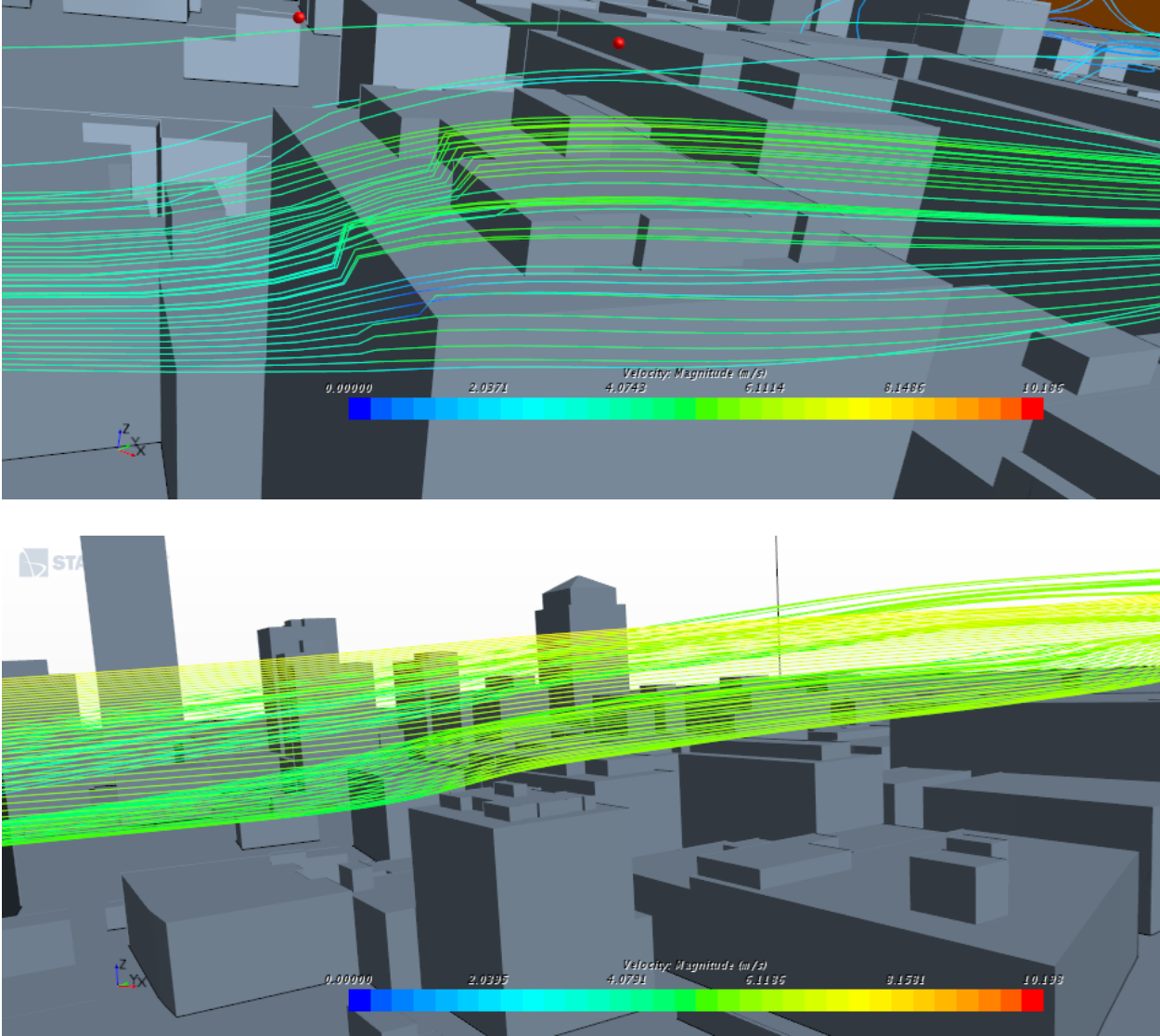
Figure 29: a) The 3D flow streamlines above the building roof top using k-epsilon Realizable model b) the same streamlines with the same location for both models, using k-epsilon Realizable model
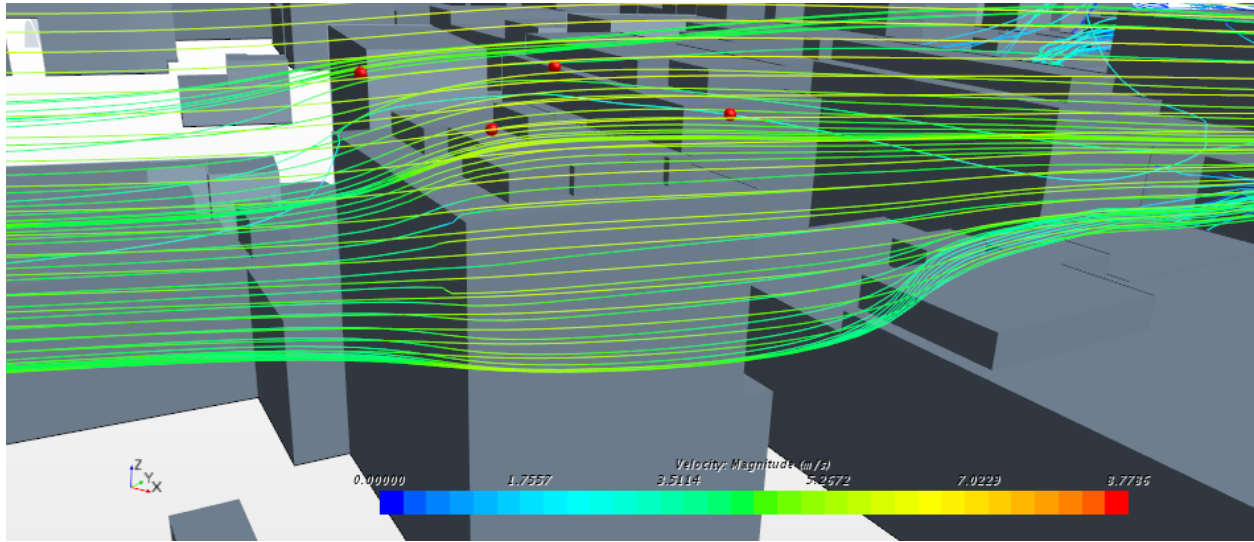
Figure 30: The 3D flow streamlines above the building roof top using k-epsilon Standard model

The streamlines around the building in both models shows the behavior of the flow moving over the building or form vortexes between the buildings, the streamlines in both models were almost the same with a slightly higher ranges for realizable model in velocity of the flow around the building. In this study, The Realizable k-epsilon model seems to be able to capture more details of the wind flow in the urban area and specially around the building.

3.3.4 Vorticity Around the Building

Another important parameter affecting the efficiency of the wind turbine is the amount of vorticity at the top of the building. As we can see in Figure 31 and Figure 32, the vorticity contours are almost the same for both models, while the K-epsilon Realizable model demonstrated higher rates of vorticity in the computational domain. Vorticity is the curl of velocity field that measures the local rotation of a fluid.
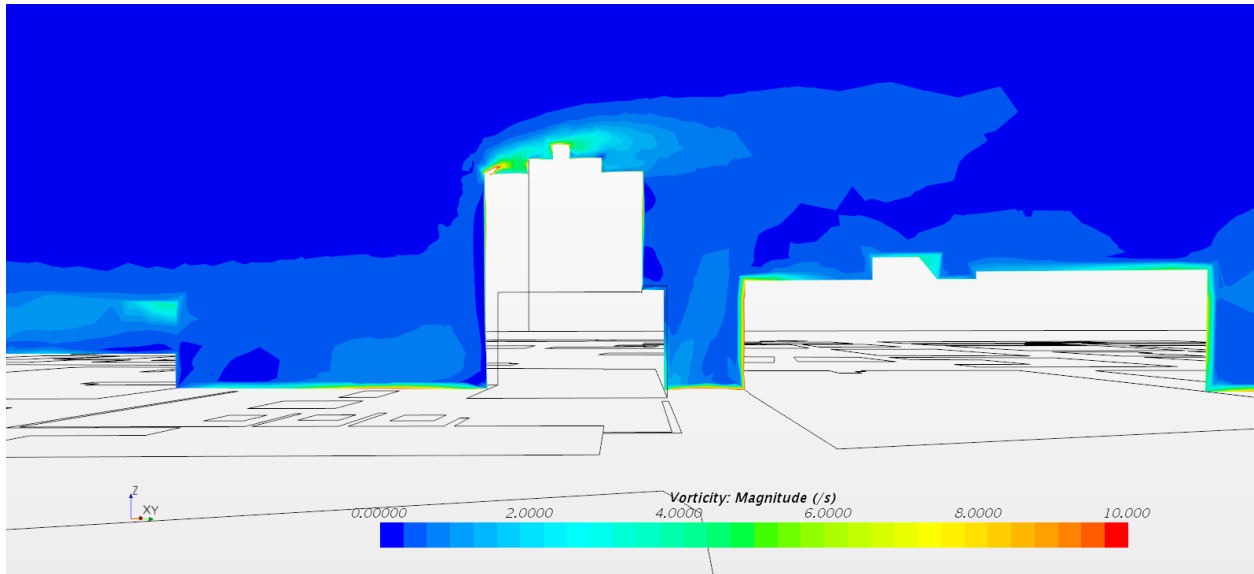
Figure 31: Vorticity (/s) above the building using k-epsilon Standard model
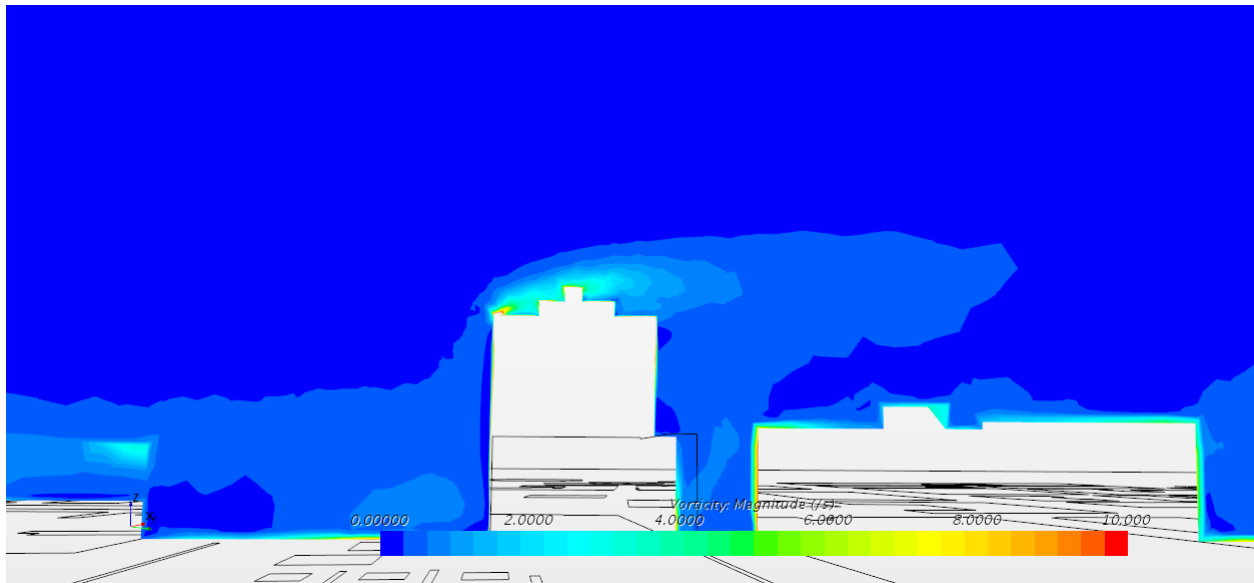
Figure 32: Vorticity (/s) above the building using k-epsilon Realizable model

3.4 Calculation of Energy output from one wind direction

The wind data Figure 33 in determined that in Montreal, the wind blows mostly from the west direction. Therefore, in both test cases, it is crucial to study the flow behavior while the wind rise from this direction. In each test case, we must illustrate the streamlines from the locations of interest and study the path of the wind flow above the building.
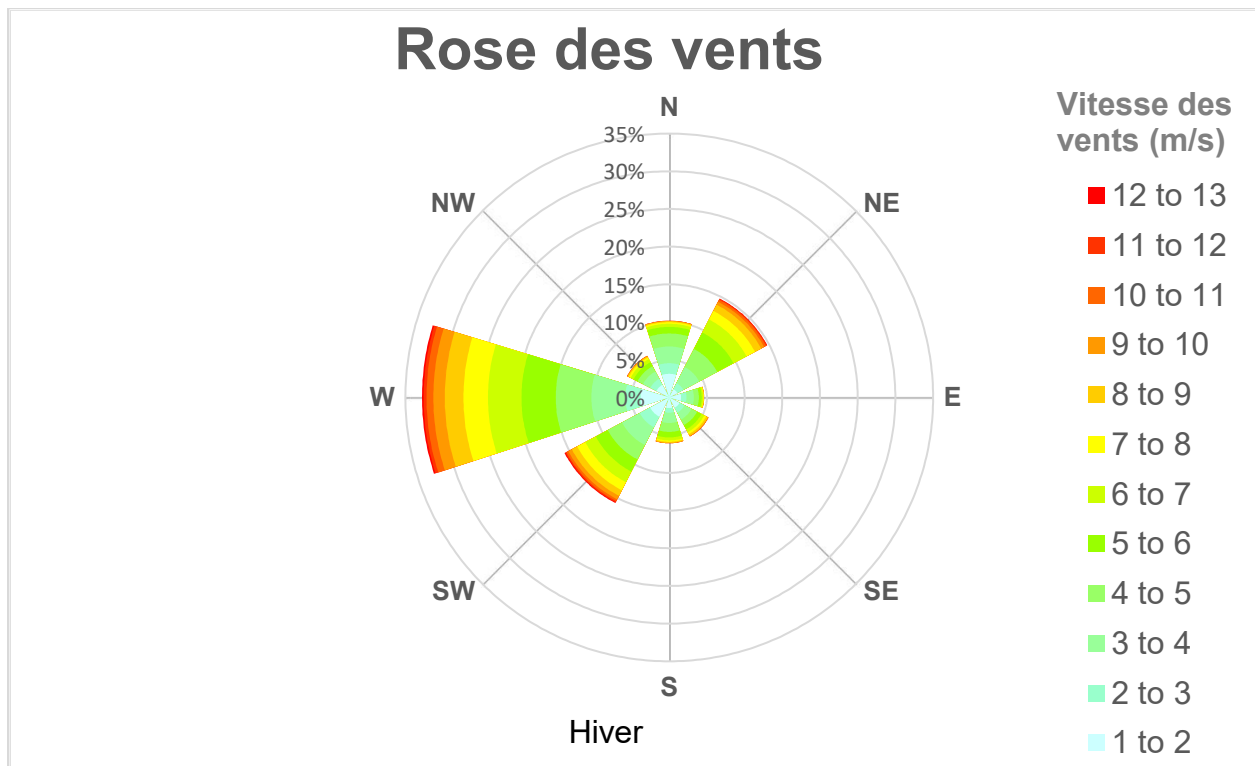
Figure 33: Wind Roses in Montreal for Winter months [45]

To investigate the power from the wind that a turbine can produce, we must estimate the velocity at the turbine location. It is known that wind power increases with the cube of wind speed, also, as we do not have the turbine already installed at the top of the building, hence, the area of the turbine

considered as unity, in other words, in this study the amount of the power per unit area is calculated. Hence the equation of wind power is written as below:

$$P_{wind} = \frac{1}{2}\rho A U^3 \qquad (11)$$

To calculate the actual amount of velocity at the top pf the building and regarding the wind capacity available from each direction, we consider seven bins as the average velocity of the wind at the inflow of 2,4,6,8,10,12 and 14 (U_{cp}) with 2m/s interval for each bin from 1-3 m/s wind speed up to 13-15 m/s wind speed. To scale the velocity which was extracted from the simulation (U_{wind}), we need to use a coefficient which is the average velocity at the inlet divided by the reference velocity at the boundary condition of the simulation which was 5m/s at 10 m height (U_{ref}), and then scale it by multiplying in incoming wind results to the actual velocity at the location of the turbine (U_{actual}). Hence, the wind velocity can be related to the hourly mean wind speed and direction.

$$U_{actual} = \frac{U_{wind}U_{cp}}{U_{ref}} \qquad (12)$$

To calculate the Energy output for the entire year, wind frequency at each velocity average bin is extracted from the meteorological data. Considering the 8760 hours in the entire year, the amount of Energy output is calculated by multiplying wind power by the total hours in the year and then scaled by the wind frequency. By dividing by 1000, this amount is converted to the scale of $KWh/_{m^2}$.

Table 4 represents the Actual velocity (m/s) and Energy output ($Wh/_{m^2}$) against each average velocity bin, taking an example of average velocity of 2 m/s, the corresponding actual velocity on the building roof and energy output are 2.80 m/s and 6912 $Wh/_{m^2}$ respectively. As illustrated, while average velocity bin grows to the right of the table, the two other variables (actual velocity and Energy) increase.

Table 4: Contribution to Estimated Energy output at point 2 from the West wind.

Average Velocity m/s	2	4	6	8	10	12	14
Actual velocity m/s	2.80	5.6	8.4	11.2	14.0	16.8	19.6
Frequency	5.83%	9.22%	9.00%	5.72%	2.43%	0.60%	0.24%
Power Watts/m^2	13.53523	108.28	365.45	866.25	1691.90	2923.61	4642.58
Energy Wh/m^2	6912	87456	288121	434055	360152	153664	97605

Energy output for each control point for one wind direction are calculated and presented in Figure 34 as illustrated, the highest total energy output value is found at location 2 (with the value of 1992 KWh/m^2), the position of point 2 is also indicated on the roof top at 5 meters above the roof in Figure 35, The other three locations (points 1,3 and 4) represent approximately the same range of annual energy output values with the average of 600 KWh/m^2 . Considering the energy values, point 2 (located on the North corner of the rooftop of building) is deemed as the best out of the four locations to install the wind turbine.
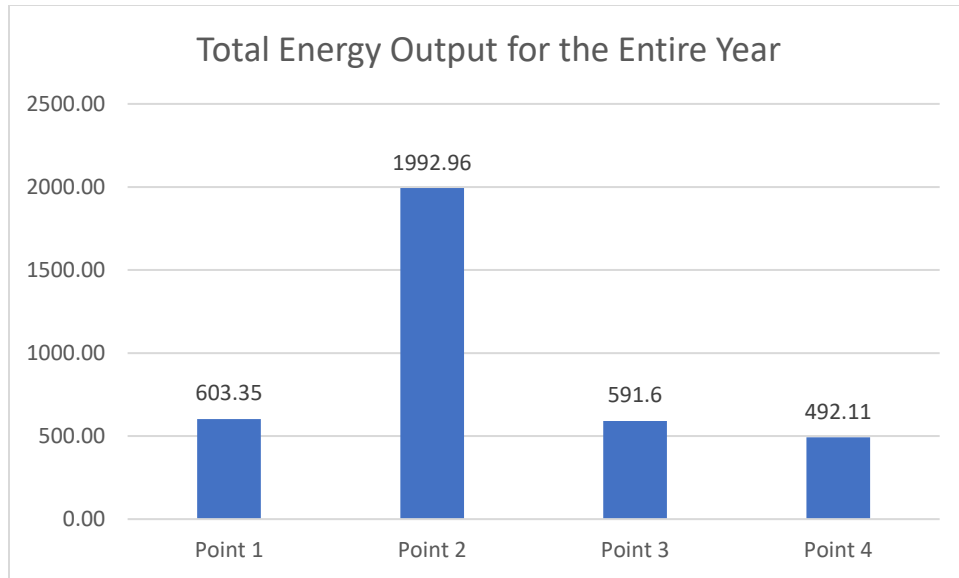
Figure 34: Energy Output for the entire year at each control point above the building from the West wind
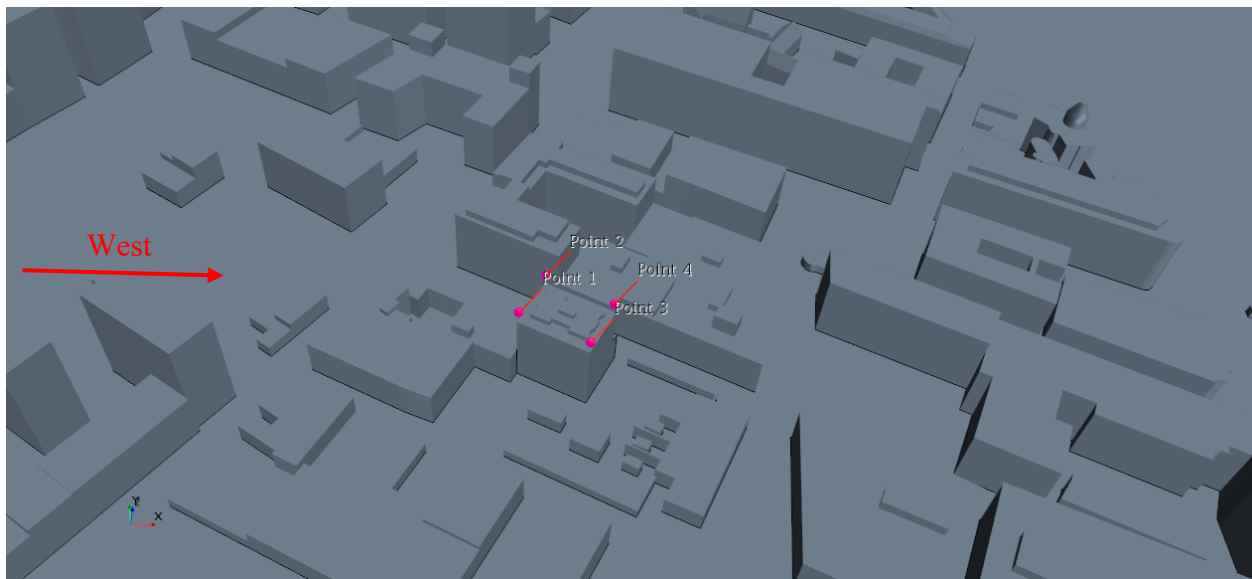
Figure 35: the location of each control point above the EV building

CHAPTER 4: Experimental comparison and validation: TEST CASE of EV BUILDING

4.1 Test Case Description

In this section the results of the wind velocity and total energy output calculations above the EV building are investigated. The points are selected at four edges of the EV building (Figure 36). The velocity at each point is evaluated for eight wind directions. The computational domain in an octagon and 8 simulations are run to calculate these velocities. Furthermore, the total energy output per unit area for each point is calculated. One of the points was analyzed previously both with actual measurements and by using wind tunnel test[32]. First, the computational results are compared with these results. Then, the potential Energy output for the entire year is calculated at each point to compare these locations so to identify the best location for the installation of wind turbines.

4.2 Geometry and Computational Domain

The geometry used for the validation is the surrounding of the EV building of Concordia University which is shown in Figure 37, The same number of surrounding buildings as the model built for experimental wind tunnel setup has been made in order to conduct a comparison with the experimental results [32]. Figure 38 shows the location of the four control points above the EV building. The total Energy output will be investigated at these four corner points of the roof top of the building. Point 3 is selected at the same location at the same location as the field measurement data above the EV building.
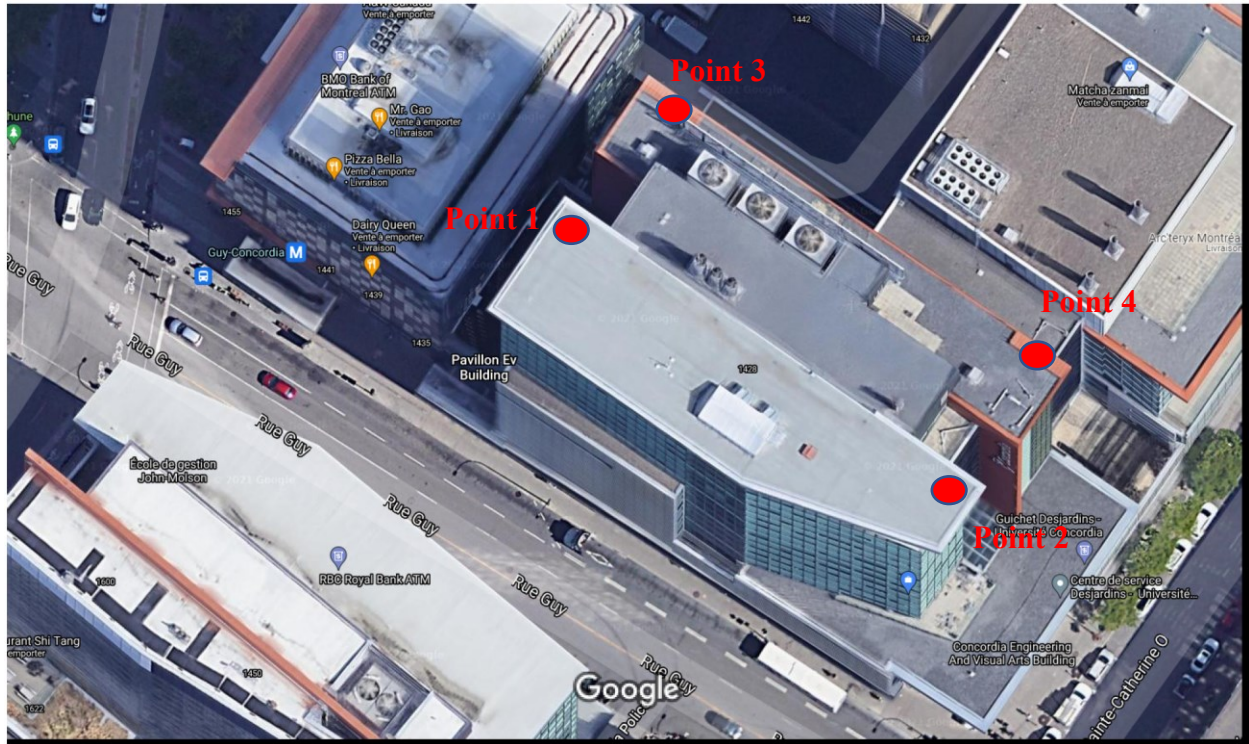
Figure 36: Location of the 4 control points above the EV rooftop
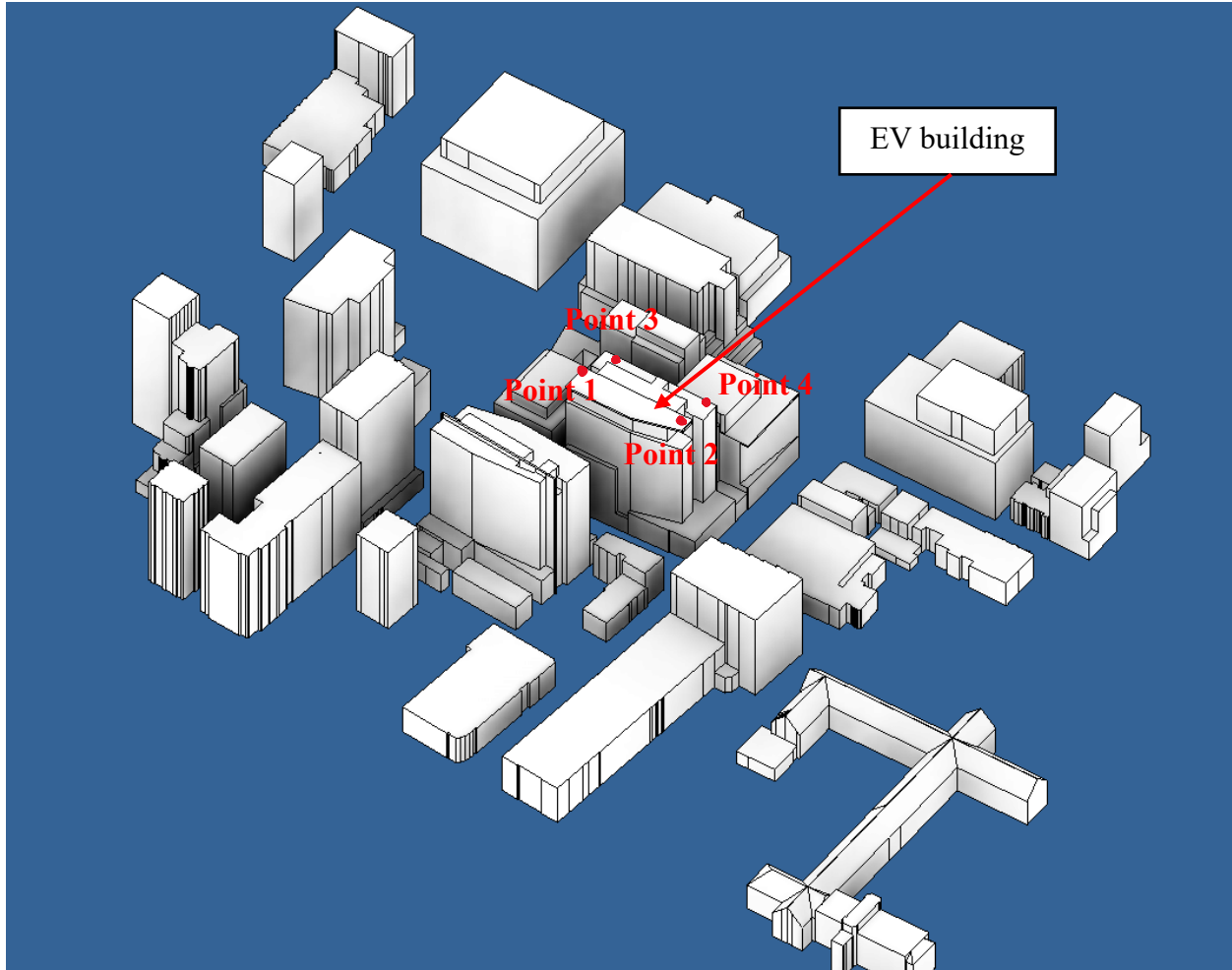
Figure 37: 3D CAD model of the geometry and the location of EV building

In Figure 38, the dimensions of the computational domain are selected as the height of the computational domain is 10 H where H is the height of the tallest building in the computational domain, also, the buildings are surrounded in an octagon [46]. The dimensions of the computational domain are taken the same as the verification section. The height of the octagon is 1000 m, and the width of the building zone is almost 1000 m, and the boundaries of the octagon are 1000 m from the edge of the building zone (Figure 39).
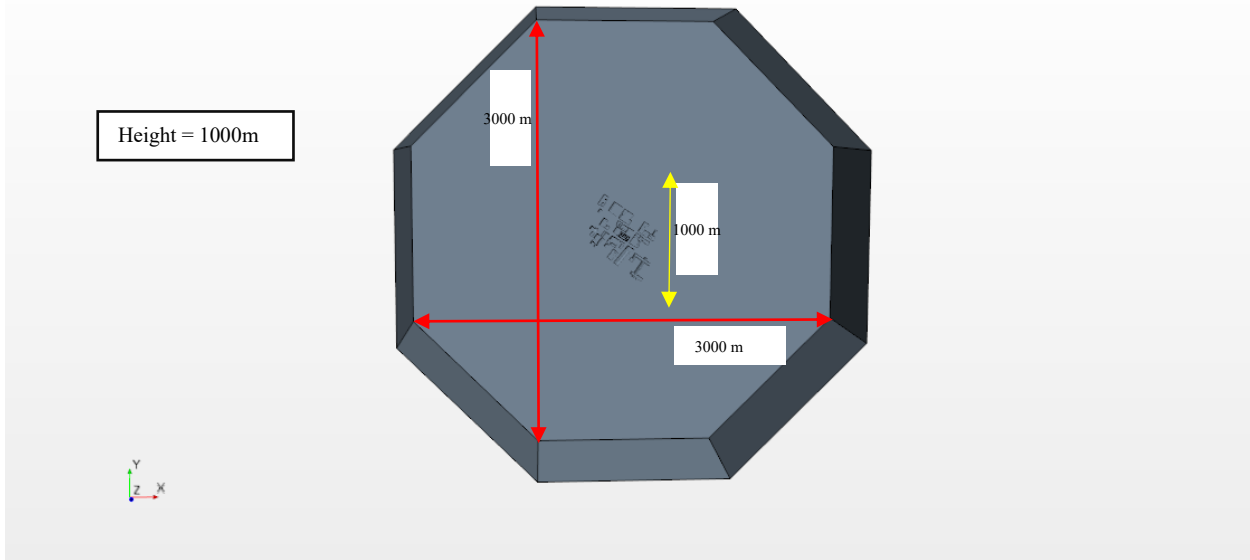
Figure 38: Isometric view of the computational domain dimensions
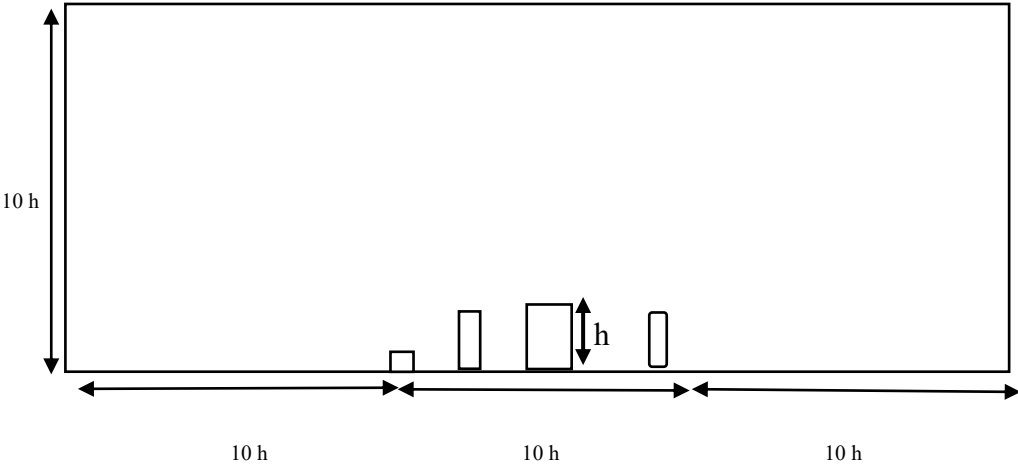
Figure 39: Isometric view of the domain for the simulation of the EV building

4.3 Mesh setup

STAR CCM+ automatic volume mesher is used to create volumetric elements with tetrahedral meshing model. The prism layer created around the buildings and specially around the EV building to capture the boundary layer flow and give more precise details above the EV building. In this case, we use 20 million mesh tetrahedral cells to provide an acceptable precision and a computational cost-effective method. 5 prism layers are executed around the EV building to capture the boundary layer and have more accurate results.
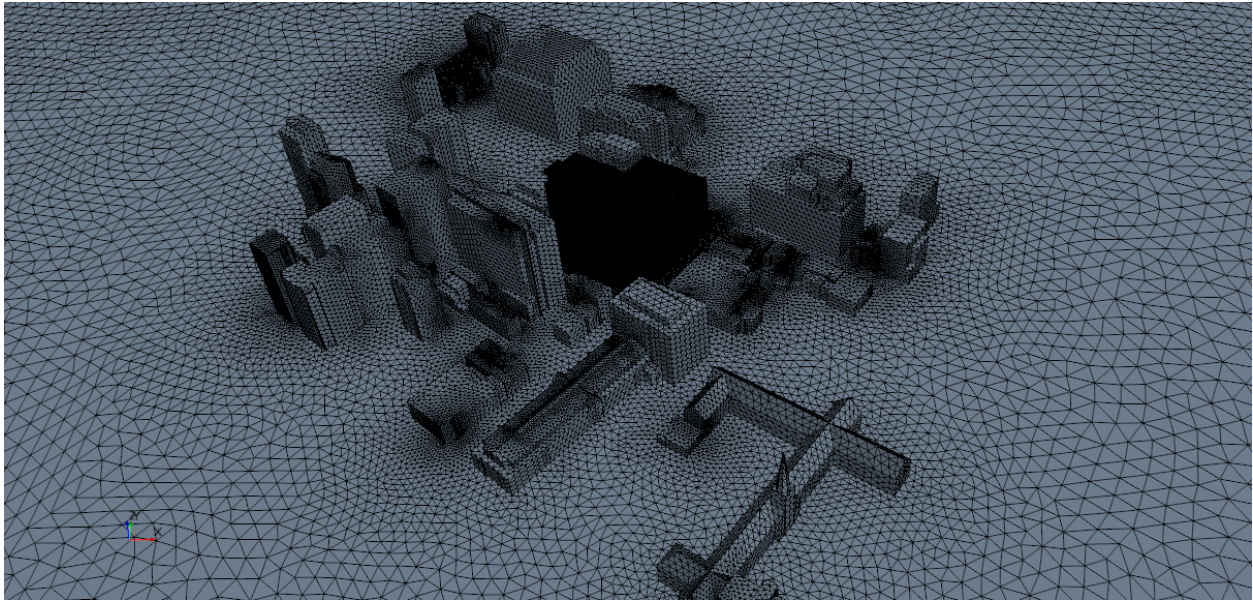
Figure 40: Surface Mesh around the EV building
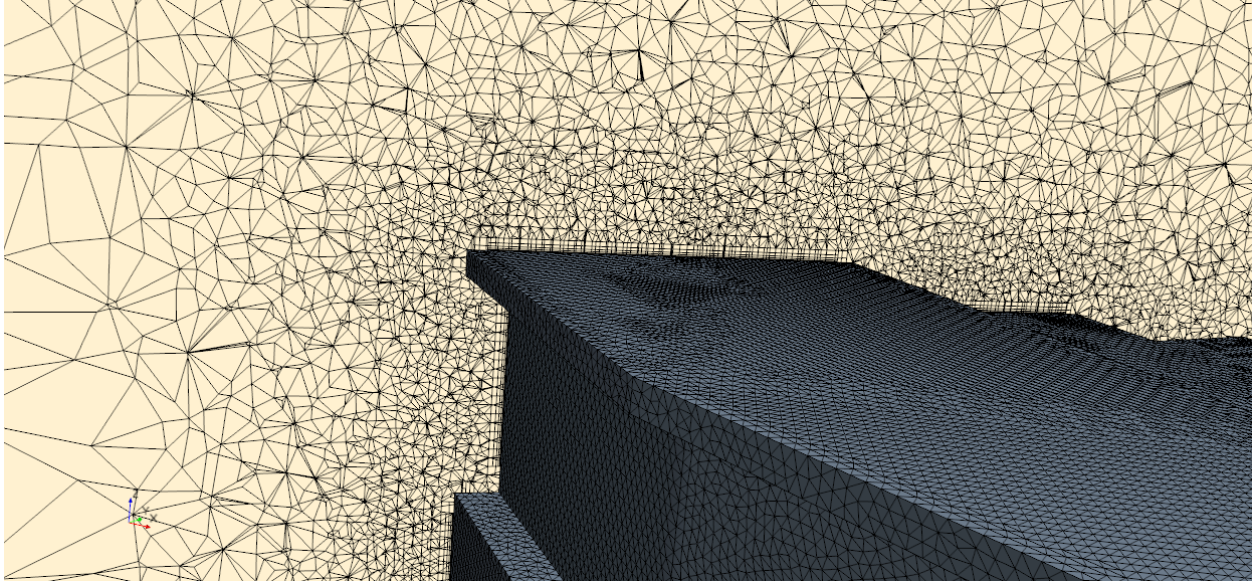
Figure 41: Prism layers round the EV building

4.4 Boundary Conditions

An octagonal computational domain is defined for this case study as 8 calculation scenarios are performed in 8 different wind directions. In this case, 8 separate simulations are conducted, each described as following; In each scenario, one specific wind direction is selected, and 3 adjacent faces exposed by that specific wind direction (Figure *42*) is considered as the inlet velocity, and the corresponding 3 opposing faces in front were selected as the outlet with the gage pressure of 0, and the other faces are set accordingly as no slip boundaries. As an example, in the test case illustrated in Figure 42, the West, North-West and South-West faces have been selected as the velocity inlet, the opposing faces, which are East, North-East, and South-East are selected as pressure outlet. The other faces (North, South) are symmetry planes, turbulent intensity of 0.1 is set as the initial condition and turbulent viscosity ratio is kept as the default value of 10 [42]. The turbulent intensity is defined as the ratio of the root-mean-square of the velocity fluctuations, to the mean flow velocity.
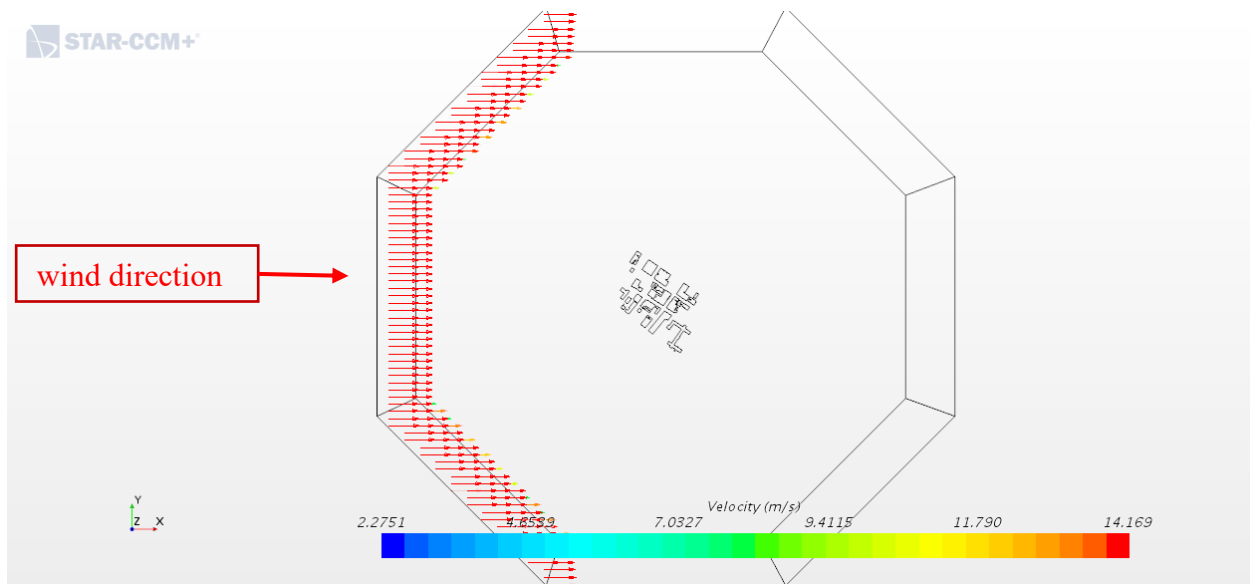
Figure 42: The inlet velocity vectors while the wind direction is considered from the West

4.5 Convergence

To study the convergence of the results, we analyzed the steady state solution for the last 800 iterations. The velocity magnitude at all 4 control points above the building is extracted for the last 800 iterations. We can report that the solution has reached the convergence and the results will not change with further computations. Figure 43 shows the velocity magnitude at the control points above the EV building while the wind is blowing from the West direction. Figure 43 demonstrates that the velocity magnitude at the location reach a stable amount around 6.2 at point 1 after 10800 iterations.

49
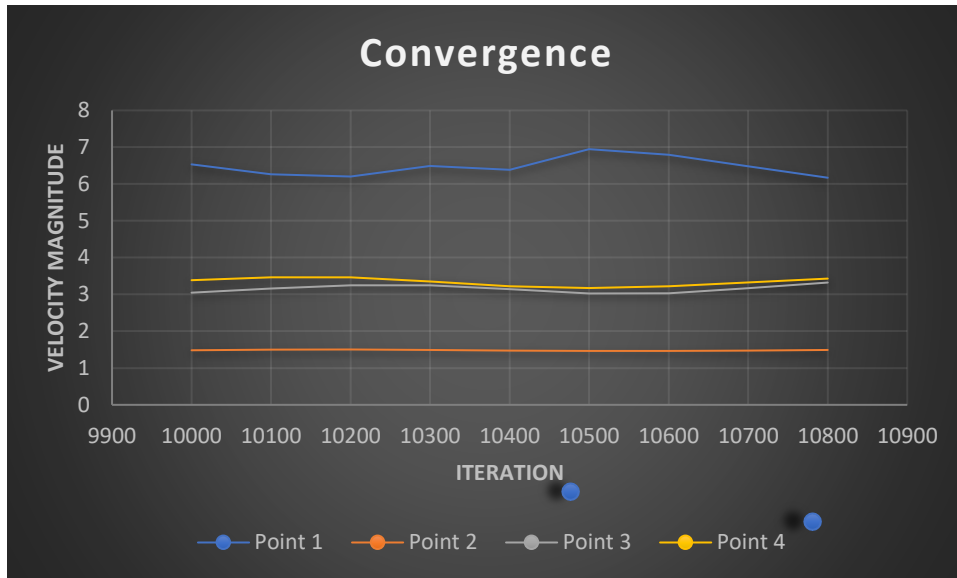
Figure 43: Velocity magnitude changes vs iterations at all control points

Note that, in the first attempt with 2 prism layers around the building the results did not converge after 11000 iterations. With 5 prism layers around the building, the simulation is converged after 11000 iterations.

4.6 Validation with field measurements

To validate results of the CFD simulation , we calculate the energy output above the EV building and compare it with field measurements [32]. Similarly, they did not consider an actual wind turbine above the EV building, the area of turbine is set as the reference area of $1 \ m^2$. The results for the total energy available are reported per unit area in this study.

The approach taken to calculate the total energy output is as follows.: the velocities corresponding to each point above the EV building are extracted from STAR CCM simulations and then the actual velocities at each control point are calculated as per the procedure described in the following paragraphs. Consequently, the total amount of energy output for the entire year has been calculated for each control point. Eventually, the point with the highest energy output value can be selected as the best location to install a turbine.

To calculate the actual velocity at each control point location, we use the average velocity in each bin, for instance, considering the average velocity of 2 m/s bin which represents the all the velocities between 1-3 m/s, for example from the West direction these velocities occur with a frequency of 5.83%. Using the scaling of Equation 12 the actual wind velocity at this point from the west related to 2 m/s is 1.35 m/s. The next step is to calculate the power output and by multiplying the power by the time and the wind frequency, the total energy available is calculated. As an example, for the West wind rose, the wind power is about 1.52 Watts/m^2 at 1.35m/s, the frequency of this wind is 5.83% so that the Energy output for this location is 778 Wh/m^2. Table 5 reports the yearly energy output results for the West wind from West at the point of interest.

Table 5: Estimated energy output on point 4 above the EV building from West direction

Average Velocity m/s	2	4	6	8	10	12	14
Actual velocity m/s	1.35	2.71	4.06	5.41	6.77	8.12	9.48
Frequency	5.83%	9.22%	9.00%	5.72%	2.43%	0.60%	0.24%
Power Watts/m^2	1.52	12.20	41.18	97.62	190.66	329.46	523.17
Energy Wh/m^2	778	9855	32468	48913	40585	17316	10999

The amount of actual velocity rise as we move in the tables from left to right because the average velocity bins get higher amounts from 2 to 14.

4.7 Energy potential estimate validation

By calculating the amount of power (per unit area as we did not consider the turbine in this study) and considering the wind velocity frequency for each average bin velocity and for each direction, in regards with the total hours that we have in the whole year, we can compute the energy output for each average bin in each direction, Figure 44 illustrates the amount of annual total Energy Output at point 3 which is about 1375 $KWh/_{m^2}$.
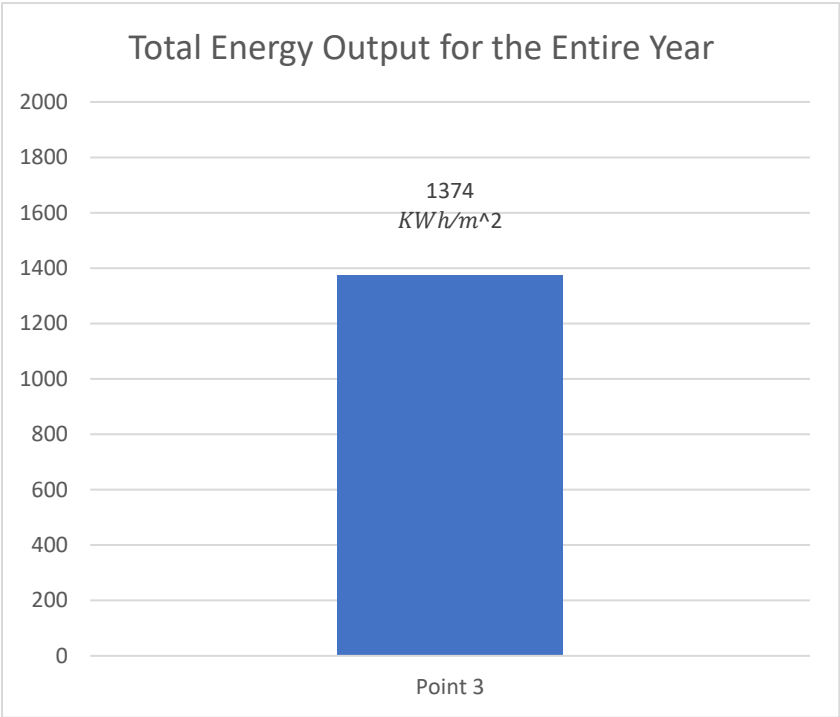
Figure 44: The total amount of energy output ($KWh/_{m^2}$) at location 3

A three-cup anemometer was installed at 2m height above the building on the North-East corner of the roof top with the purpose of calculating the wind energy with field measurements data. The anemometer's frequency was set to capture the data every 5 seconds for the duration of August

2013 to October 2013 and the data gathered was in turn used to calculate the total wind energy for the mentioned period. Figure 45 provides the field measurement data(in black and white) and the Estimated value (in blue) of the potential energy output for the year [32]. It shows that the amount of the total wind energy per unit area for the entire year with the data collected from August to October 2013 (black bars in Figure 45). Figure 46 shows the exact location of which the anemometer was installed.
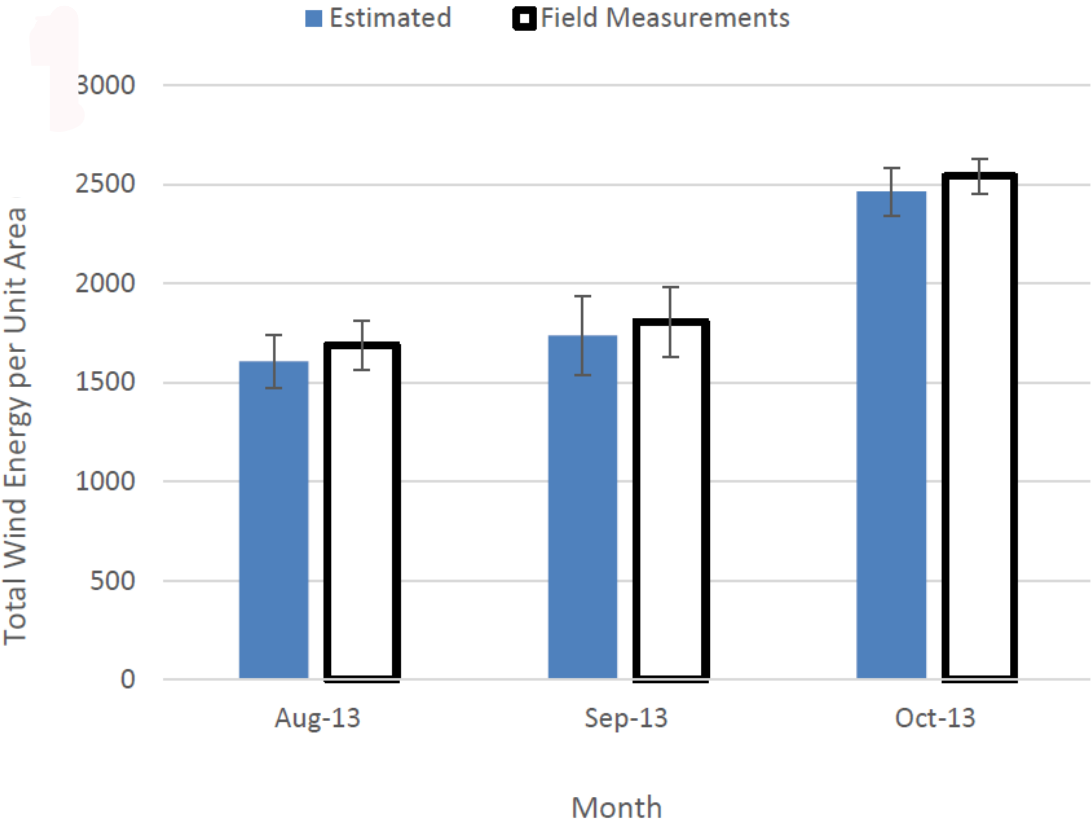
Figure 45: Field Measurement Data and the Estimated Values above the Roof of EV Building with the Corresponding Error Bars. [32]

Figure 46: The Location for the anemometer in Al-Quran study

With comparing the amount of energy output that we calculated with the numerical method with the amount of energy output estimated from the field measurement data in Al-Quran case, it is demonstrated that the amount of the energy output extracted from simulation in STAR CCM+, is slightly lower than what they estimated by field measurement. When comparing our result with the estimated wind tunnel results, we need to take into consideration that the wind rose used as reference in the wind tunnel estimate study above EV building at point 3 is as Figure 47 (a). Note that in Al Quran case, the dominant wind direction is West and South-West, however in our case, the reference Wind Rose is as Figure 47 (b), which indicated the West direction is the dominant wind direction. Moreover, in Al-Quran study, 16 different directions are considered to specify the frequency of wind direction (for instance, the West-South-West has about 13% of frequency), while in our study, we took 8 different directions and 8 corresponding simulations. The total Energy output at point 3 from the measurement field with anemometer above the EV building is about $2100 \, ^{kWh}/_{m^2}$, while the estimated amount for the energy output from the wind tunnel data is about $1900 \, k \, ^{Wh}/_{m^2}$ and in this case using STAR CCM+ tool, it is slightly lower about $1375 \, ^{kWh}/_{m^2}$

.
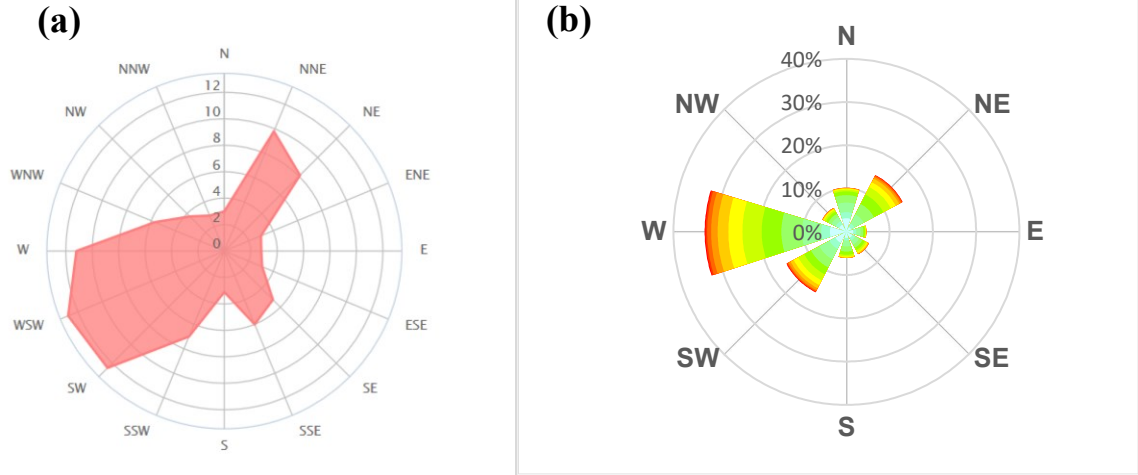
Figure 47: a)Yearly Wind Rose of Montreal (Wind Direction Distribution in %)[47] b) Wind Rose in Montreal in Winter months (Wind direction Distribution is in %)

It is obvious that the amounts calculated for the total energy output are different, specifically, while the dominant wind rose in our case is mostly West direction, however the dominant wind rose in Al-Quran case was West and South-West. The proposed methodology is under predicting the amount of energy output at location 3 in comparison with estimated data from the wind tunnel but as discussed, these results are very sensitive to the meteorological data used.

Chapter 5: Energy Output Analysis

After comparing energy output at point 3 with other results we now focus on all 4 points to identify a potential best location to install a wind turbine. The main reason behind selecting the aforementioned points, was the orientation of the EV building and hence, the associated exposure of these individual points to the West and South-West wind directions. In Figure *48*, Point 1 and 2 have almost the same energy output potential (about 2300 KWh/m^2), point 3, has the lowest energy output potential among all 4 control points which is about 1374 KWh/m^2 , this could be due to the location of this point at the rooftop which could result to the low exposure to the wind.
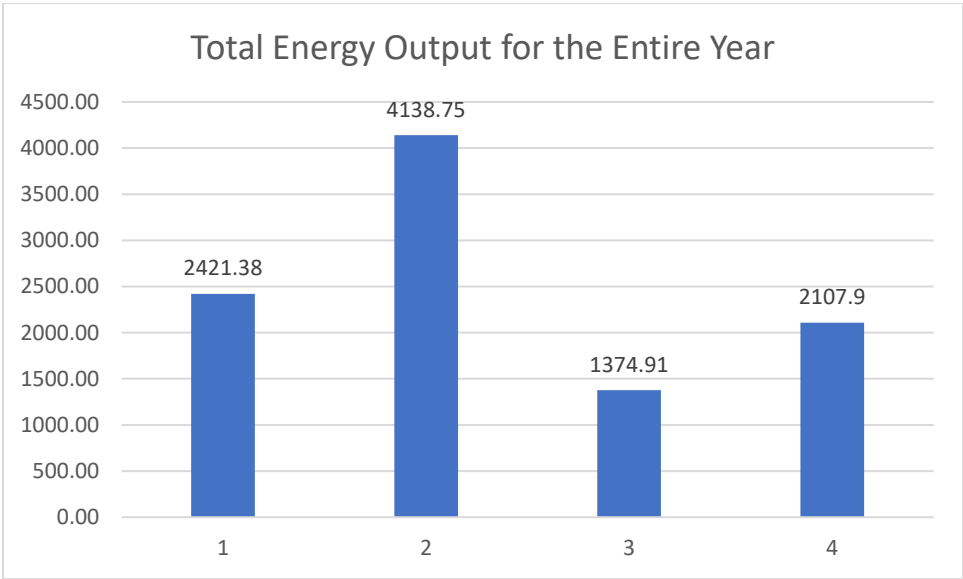
Figure 48: The total amount of energy output (KWh/m^2)

The above histogram (Figure *48*) illustrates the distribution of total energy output for the entire year for each point 1, 2, 3 and 4. As indicated, point 2, has the highest amount of cumulative energy output for the entire year (4138.75 KWh/m^2). Figure *49* shows the position of the point 2 and the exposure that this point has to the West wind direction.
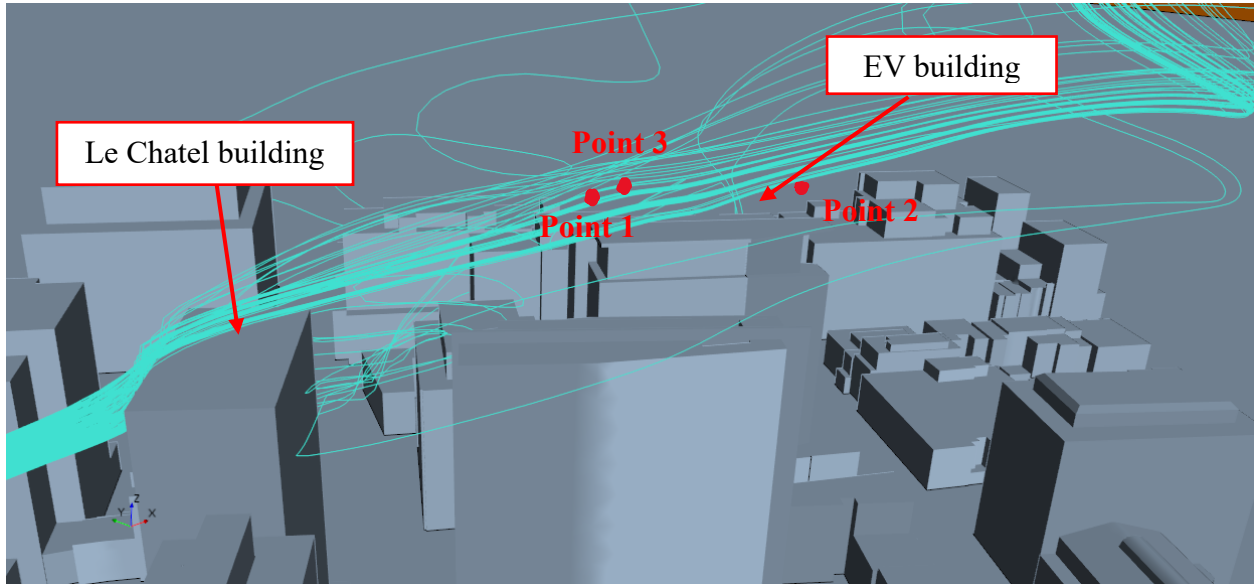
Figure 49: The wind flow behavior above the EV building

.

5.1 Discussion and Analysis of Energy Potential and flow over the building at all control points

The data extracted from the simulation demonstrates a noticeable low amount of velocity magnitude at the EV location while the wind is blowing from the South-West direction. As discussed before, in Al-Quran study the West and South-west are two principal directions regarding the wind rose table in Montreal, but in this study, only West direction is the dominant direction for the wind flow, Hence, the wind velocity and energy output are shown in following tables considering the two West and South-West wind direction for comparison purposes at point 1, 2 and 4. Table 6 and Table 7 are providing the data on actual velocity and energy output at location of point 1 from South-West wind and West wind respectively.

Table 6: Estimated energy output for point 1 above the EV building from South-West direction

Average Velocity m/s	2	4	6	8	10	12	14

Actual velocity m/s	0.10	0.21	0.32	0.43	0.54	0.64	0.75
Power Watts/m²	0.000758	0.01	0.02	0.05	0.09	0.16	0.26
Frequency	4.43%	4.80%	3.38%	2.03%	0.80%	0.28%	0.14%
Energy Wh/m^2	0.29	2.55	6.06	8.62	6.64	4.01	3.19

Table 7: Estimated energy output for point 1 above the EV building from West direction

Average Velocity m/s	2	4	6	8	10	12	14
Actual velocity m/s	2.61	5.23	7.84	10.46	13.07	15.68	18.30
Power Watts/m²	10.98	87.88	296.59	703.03	1373.10	2372.72	3767.78
Frequency	5.83%	9.22%	9.00%	5.72%	2.43%	0.60%	0.24%
Energy Wh/m^2	5610	70976	233831	352267	292288	124709	79213

Considering the wind velocity frequency of 9% from West direction at 6 m/s average velocity, the energy output is about 70 KWh/m^2 , In comparison, we can find much less of energy output from the same location considering the wind direction from South-West at the same average velocity of 6m/s, as the wind frequency from this direction is about 4.8%.

Table 8: Estimated energy output for point 2 above the EV building from South-West direction

Average Velocity m/s	2	4	6	8	10	12	14
Actual velocity m/s	1.35	2.70	4.06	5.41	6.76	8.11	9.46
Frequency	4.43%	4.80%	3.38%	2.03%	0.80%	0.28%	0.14%
Power Watts/m^2	1.51	12.16	41.04	97.27	189.98	328.29	521.31
Energy $Wh/_{m^2}$	589	5112	12150	17297	13314	8052	6393

Table 9: Estimated energy output for point 2 above the EV building from West direction

Average Velocity m/s	2	4	6	8	10	12	14
Actual velocity m/s	0.59	1.19	1.78	2.37	2.97	3.56	4.15
Power Watts/m^2	0.12	1.03	3.47	8.22	16.05	27.73	44.03
Frequency	5.83%	9.22%	9.00%	5.72%	2.43%	0.60%	0.24%
Energy $Wh/_{m^2}$	65	829	2732	4116	3415	1457	925

In Table 9 while the wind flow is from West direction, in the average velocity of 6 m/s bin, we have 1.78 m/s of actual velocity. With considering the wind frequency of 9.0%, the energy output that we can exert from the wind turbine which is located at 2 meters above the EV building in the east corner of the EV building is about 2732 $Wh/_{m^2}$ .This amount for energy value is less than 12150 $Wh/_{m^2}$ when the wind blows from the South-West direction as reported in Table 8 . This

could be due to the exposure of the point 2 to the West and South-West wind direction, to better analyze this occurrence, we need to study the wind flow over the EV building in Figure *50*.
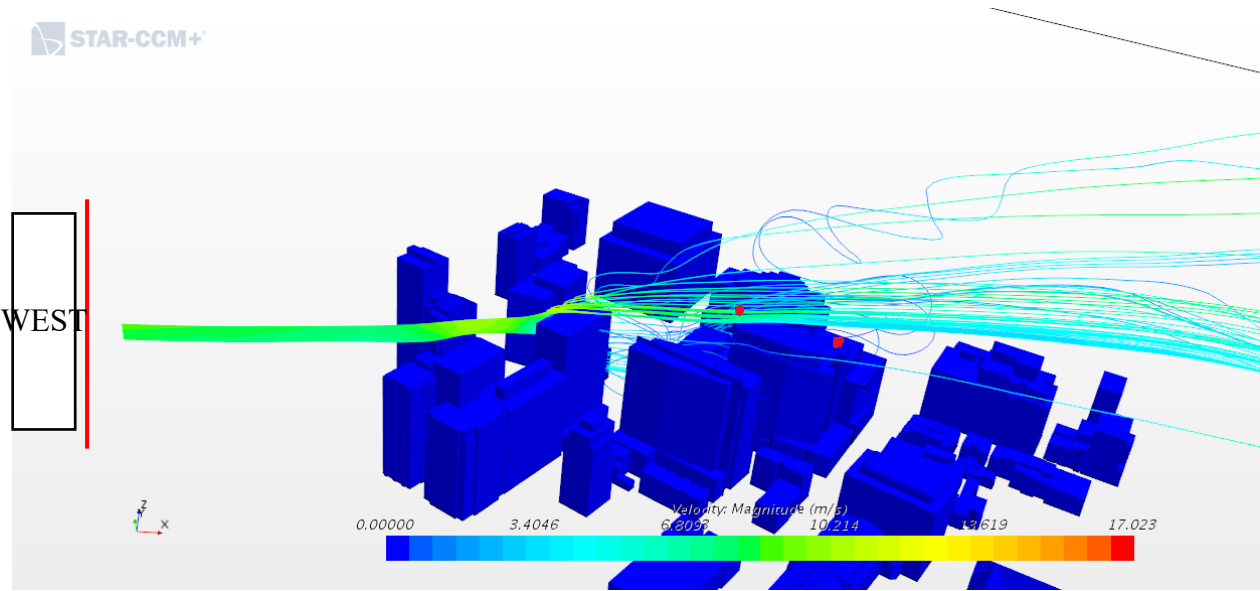
Figure 50: The flow streamlines while the wind rose from West direction

Hereby, we investigate the flow behavior in this situation to study the reason behind this amount of velocity magnitude at the roof top while we apply the wind rose from the West boundary condition. Figure *50* Demonstrates some streamlines and their path through the buildings from the top view.

When we have a closer view of the streamlines which blown from the West and their path through the EV roof top, it is obvious that there is a higher building (Le Chatel) at the west side of the EV

60

building which blocks the wind path through The EV building. Figure 51 shows the streamlines hit the Chatel building before they reach to the EV building, thus the associated values for velocity magnitude while the wind is rise from the west direction are low although the frequency of wind rose from the West has higher percentage comparing with other directions.
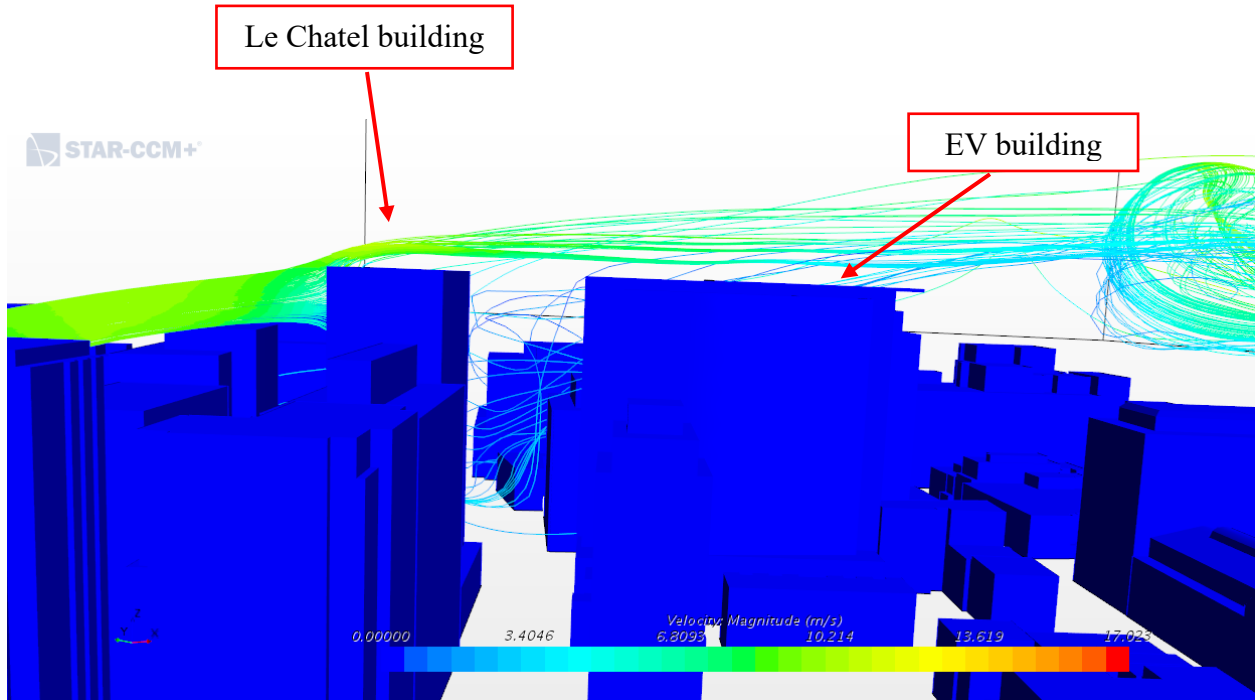
Figure 51: The wind flow above the buildings while the streamlines are redirected as they pass through the Chatel building

As indicated in Figure 51, it is observed that the streamline pattern and distribution of the wind streamlines above the Chatel and EV building, points 2 and 4 are exposed to higher magnitude of wind flow from West and South-West and higher total value of Energy are expected at these locations. The exposure of this point could result into increase in the velocity magnitude and the energy output at this point. Studying the flow from the West direction is particularly important as it has the most frequency percentage in Montreal (Figure *33*).
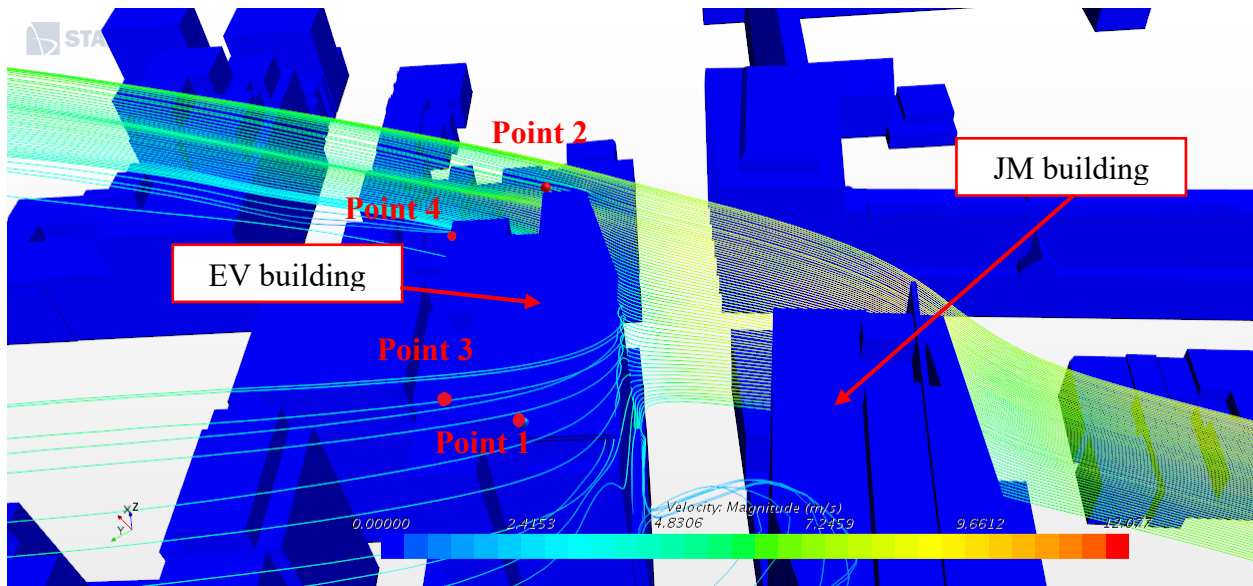
Figure 52: The streamlines behavior while reaching the EV building and the location of the three control points

Figure 52 explains why the velocity magnitude has lower amount at point 1 comparing to point 2 when the wind inlet is from the South-West direction. While we study the wind rose from the South-West direction, the wind blows from the inlet (South-West) and before it reaches to the EV building, it will hit the John Molson Building (JM Building), most of the streamlines continue their path through point 2 at the East Corner of the EV roof top (green and orange streamlines) and only a small proportion of the streamlines seem to find their way through the point 1 at the West corner of the EV roof top with lower amounts of velocity magnitude (Blue streamlines). The exact amount of the velocity magnitude at these points are reported at Table 6 and Table 8.
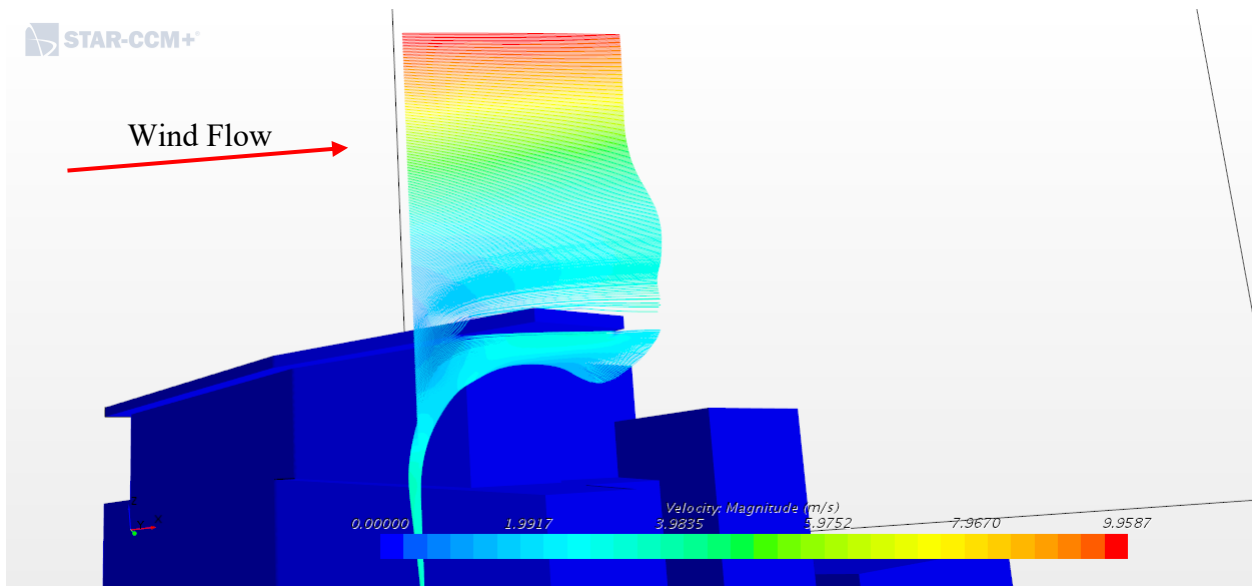
Figure 53: The flow field around the EV roof top
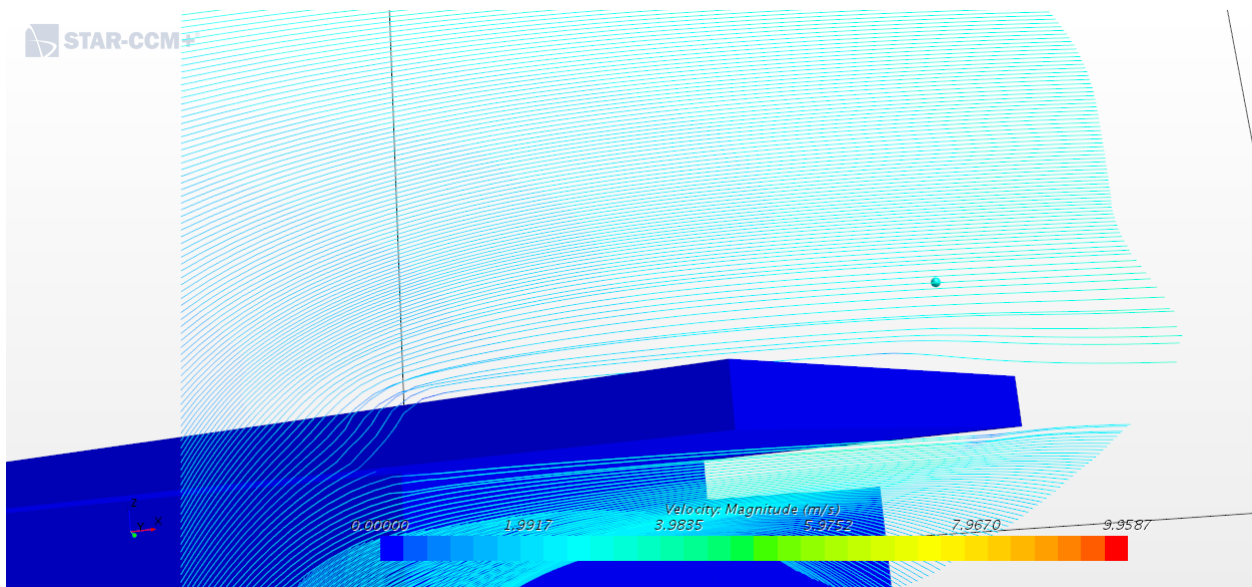
Figure 54: The streamlines behavior over the roof top of the EV building around point 2

The flow field around the EV building is studied and the flow field near the EV building rooftop is shown in Figure 54. The position of the control point 2 is shown in this figure and the velocity magnitude of the wind blowing from the West toward point 2 is demonstrated.

With observing the wind flow over the EV building and the flow streamlines extracted from STAR CCM+, the forth point added at the NE corner of the building, the amount of velocity at location point 4 and the Total Energy Output is as below, it is shown that this point has the same potential of Wind Energy Output as point 1 (Figure *37*).

Table 10: Estimated energy output for point 4 above the EV building from West direction

Average Velocity m/s	2	4	6	8	10	12	14
Actual velocity m/s	1.3536	2.71	4.06	5.41	6.77	8.12	9.48
Power Watts/m^2	1.525268	12.20	41.18	97.62	190.66	329.46	523.17
Frequency	5.83%	9.22%	9.00%	5.72%	2.43%	0.60%	0.24%
Energy Wh/m^2	778	9855	32468	48913	40585	17316	10999

CHAPTER 6: CONCLUSION AND FUTURE WORK

6.1 Concluding Remarks

This study provides a methodology using CFD to evaluate the potential energy of roof mounted turbines in urban areas. A case study of the potential energy output at the roof top of downtown building (EV building) is presented and the results are first compared with experimental data in the wind tunnel and the analysis is expanded to evaluated different positions to place a wind turbine.

Since the numerical method needs to offer an accurate and cost-efficient approach to study the flow, the mesh is investigated to achieve with the smallest number of cells for an acceptable accuracy. In order to achieve mesh independent results, three different meshes around a building located on King street are studied. Results with a mesh containing 10 million elements were acceptable due to the accuracy and the computational cost for running the simulations of the flow over buildings. Hence, the values of the velocity at 4 control points did not change significantly between the two finest meshes. To validate the methodology, a case study of a EV building was studies. Results are compared with the experimental field measurement data and wind tunnel data. The total energy output value was lower but quite in agreement with the experimental data.

As the energy output is sensitive to the wind direction and frequency, the different wind roses used in this study and Al-Quran's study may explain the differences between the total energy output at location 3 from the present calculations and estimated energy output from the wind tunnel data. In the present study, only the West wind direction is dominant while in Al-Quran's work, the West and South-West wind were dominant directions.

In summary, installing anemometer to extract the field measurement data directly at multiple locations may be an expensive approach to evaluate different locations for installing turbines. However, employing the CFD combined with meteorological data approach can easily evaluate multiple locations with different wind exposures. By studying each point, we can investigate the potential of each location in terms of annual energy output and wind velocity. Considering the duration of data recording with anemometer to extract the field measurement data which could

take months, CFD introduces a method which we could have access to the data within days and we can estimate the total year energy output. The main contribution of this work is that it can study multiple locations above the building much faster (within a month) than existing experimental methods.

6.2 Future Work

The following assumptions have been made in this study:

- We consider a constant amount for the exponent factor for the urban terrain as $\alpha = 0.31$.
- The amount of turbulent intensity is considered 0.1% which is low.
- The wind Rose data is related to only winter months.
- The linear scaling of the actual velocity to match the meteorological data is used.

Clearly, the impact of the above assumptions can be studied to evaluate the accuracy of the methodology proposed. This can be done by further investigate the EV building test case.

More specifically, the field measurements were taken during specific months in 2013. Metrological data for these exact months could be found and used the estimate energy for these specific months. This approach should provide a much better comparison with less dependence on the Metrological wind data.

Moreover, using CFD we can simulate a wind turbine at any or all control points above the nominated buildings. Different levels of accuracy can be used ranging from a steady model of the wind turbine to a full unsteady model of an actual turbine. The advantage of including the turbine in the CFD simulation is to capture the synergy between the building and the turbine as well as the surrounding buildings. Adding a steady state turbine model in the current CFD should be a little more expensive computationally than the proposed methodology but can provide significant useful information.

References

[1]   V. Nelson and K. Starcher, *Wind energy: renewable energy and the environment*. CRC press, 2018.

[2]   F. Version, "Ealing Urban Wind Study," 2003.

[3]   B. Blocken, "Computational Fluid Dynamics for urban physics: Importance, scales, possibilities, limitations and ten tips and tricks towards accurate and reliable simulations," *Build. Environ.*, vol. 91, pp. 219–245, 2015, doi: 10.1016/j.buildenv.2015.02.015.

[4]   GWEC, "Global Wind Report annual market update," *Wind energy Technol.*, no. April, p. 76, 2015, [Online]. Available: http://www.gwec.net/global-figures/wind-energy-global-status/.

[5]   D. Micallef and G. Van Bussel, "A review of urban wind energy research: Aerodynamics and other challenges," *Energies*, vol. 11, no. 9, pp. 1–27, 2018, doi: 10.3390/en11092204.

[6]   M. Zabarjad Shiraz, A. Dilimulati, and M. Paraschivoiu, "Wind power potential assessment of roof mounted wind turbines in cities," *Sustain. Cities Soc.*, vol. 53, no. October 2019, p. 101905, 2020, doi: 10.1016/j.scs.2019.101905.

[7]   T. Stathopoulos, H. Alrawashdeh, A. Al-Quraan, B. Blocken, A. Dilimulati, M. Paraschivoiu, P. Pilay,"Urban wind energy: Some views on potential and challenges," *J. Wind Eng. Ind. Aerodyn.*, vol. 179, no. August 2017, pp. 146–157, 2018, doi: 10.1016/j.jweia.2018.05.018.

[8]   T. Sharpe and G. Proven, "Crossflex: Concept and early development of a true building integrated wind turbine," *Energy Build.*, vol. 42, no. 12, pp. 2365–2375, 2010, doi:

10.1016/j.enbuild.2010.07.032.

[9]   S. Mertens, "Wind Energy in the Built Environment - concentrator effects of buildings,"
        Wind Eng., vol. 30, Oct. 2006, doi: 10.1260/030952406779502623.

[10]   L. Lu and K. Y. Ip, "Investigation on the feasibility and enhancement methods of wind
        power utilization in high-rise buildings of Hong Kong," *Renew. Sustain. Energy Rev.*, vol.
        13, no. 2, pp. 450–461, 2009, doi: 10.1016/j.rser.2007.11.013.

[11]   N. Mithraratne, "Roof-top wind turbines for microgeneration in urban houses in New
        Zealand," *Energy Build.*, vol. 41, no. 10, pp. 1013–1018, 2009, doi:
        10.1016/j.enbuild.2009.05.003.

[12]   B. Safari and J. Gasore, "A statistical investigation of wind characteristics and wind
        energy potential based on the Weibull and Rayleigh models in Rwanda," *Renew. Energy*,
        vol. 35, no. 12, pp. 2874–2880, 2010, doi: 10.1016/j.renene.2010.04.032.

[13]   I. Abohela, N. Hamza, and S. Dudek, "Effect of roof shape, wind direction, building height
        and urban configuration on the energy yield and positioning of roof mounted wind
        turbines," *Renew. Energy*, vol. 50, pp. 1106–1118, 2013, doi:
        10.1016/j.renene.2012.08.068.

[14]   "Environnement et Changement climatique Canada - Atlas éolien et données historiques
        modélisées / Environment and Climate Change Canada - Wind Atlas and Modelled
        Historical Data." http://www.windatlas.ca/ (accessed Nov. 03, 2020).

[15]   T. F. Ishugah, Y. Li, R. Z. Wang, and J. K. Kiplagat, "Advances in wind energy resource
        exploitation in urban environment: A review," *Renew. Sustain. Energy Rev.*, vol. 37, pp.
        613–626, 2014, doi: 10.1016/j.rser.2014.05.053.

[16]   D. Bobrova, "Building-integrated wind turbines in the aspect of architectural shaping,"
        Procedia Eng., vol. 117, no. 1, pp. 404–410, 2015, doi: 10.1016/j.proeng.2015.08.185.

[17]   S. Mathew, K. P. Pandey, and A. Kumar.V, "Analysis of wind regimes for energy
        estimation," *Renew. Energy*, vol. 25, no. 3, pp. 381–399, 2002, doi: 10.1016/S0960-

1481(01)00063-5.

[18]   W. T. Chong, A. Fazlizan, S. C. Poh, K. C. Pan, W. P. Hew, and F. B. Hsiao, "The design, simulation and testing of an urban vertical axis wind turbine with the omni-direction-guide-vane," *Appl. Energy*, vol. 112, pp. 601–609, 2013, doi: 10.1016/j.apenergy.2012.12.064.

[19]   A. S. Saad, I. I. El-Sharkawy, S. Ookawara, and M. Ahmed, "Performance enhancement of twisted-bladed Savonius vertical axis wind turbines," *Energy Convers. Manag.*, vol. 209, no. March, p. 112673, 2020, doi: 10.1016/j.enconman.2020.112673.

[20]   B. Wang, L. D. Cot, L. Adolphe, S. Geoffroy, and S. Sun, "Cross indicator analysis between wind energy potential and urban morphology," *Renew. Energy*, vol. 113, pp. 989–1006, 2017, doi: 10.1016/j.renene.2017.06.057.

[21]   J. T. Millward-Hopkins, A. S. Tomlin, L. Ma, D. B. Ingham, and M. Pourkashanian, "Assessing the potential of urban wind energy in a major UK city using an analytical model," *Renew. Energy*, vol. 60, pp. 701–710, 2013, doi: 10.1016/j.renene.2013.06.020.

[22]   A. Dilimulati, T. Stathopoulos, and M. Paraschivoiu, "Wind turbine designs for urban applications: A case study of shrouded diffuser casing for turbines," *J. Wind Eng. Ind. Aerodyn.*, vol. 175, no. January, pp. 179–192, 2018, doi: 10.1016/j.jweia.2018.01.003.

[23]   B. Akay, D. Ragni, C. S. Ferreira, and G. J. W. Van Bussel, "Investigation of the root flow in a Horizontal Axis," *Wind Energy*, no. February, pp. 1–20, 2013, doi: 10.1002/we.

[24]   B. Wang, L. D. Cot, L. Adolphe, S. Geoffroy, and J. Morchain, "Estimation of wind energy over roof of two perpendicular buildings," *Energy Build.*, vol. 88, no. 2015, pp. 57–67, 2016, doi: 10.1016/j.enbuild.2014.11.072.

[25]   M. Zubialde-elzaurdia, F. Lucas, and A. Bastide, "Using CFD simulation to improve estimation of wind pressure coefficient for naturally-ventilated buildings in tropical climate."

[26]   A. Khanjari, E. Mahmoodi, and M. H. Ahmadi, "Energy and exergy analyzing of a wind

turbine in free stream and wind tunnel in CFD domain based on actuator disc technique," *Renew. Energy*, vol. 160, pp. 231–249, 2020, doi: 10.1016/j.renene.2020.05.183.

[27]   T. Uchida, "Design Wind Speed Evaluation Technique in Wind Turbine Installation Point by Using the Meteorological and CFD Models," *J. Flow Control. Meas. & Vis.*, vol. 06, no. 03, pp. 168–184, 2018, doi: 10.4236/jfcmv.2018.63014.

[28]   H. Daaou Nedjari, O. Guerri, and M. Saighi, "CFD wind turbines wake assessment in complex topography," *Energy Convers. Manag.*, vol. 138, pp. 224–236, 2017, doi: 10.1016/j.enconman.2017.01.070.

[29]   F. Toja-Silva, A. Colmenar-Santos, and M. Castro-Gil, "Urban wind energy exploitation systems: Behaviour under multidirectional flow conditions - Opportunities and challenges," *Renew. Sustain. Energy Rev.*, vol. 24, pp. 364–378, 2013, doi: 10.1016/j.rser.2013.03.052.

[30]   M. A. Allard, "Performance and Wake Analysis of a Darrieus Wind Turbine on the Roof of a Building using CFD," no. December, 2020.

[31]   B. Blocken, T. Stathopoulos, and J. P. A. J. van Beeck, "Pedestrian-level wind conditions around buildings: Review of wind-tunnel and CFD techniques and their accuracy for wind comfort assessment," *Build. Environ.*, vol. 100, pp. 50–81, 2016, doi: 10.1016/j.buildenv.2016.02.004.

[32]   A. Al-Quraan, T. Stathopoulos, and P. Pillay, "Comparison of wind tunnel and on site measurements for urban wind energy estimation of potential yield," *J. Wind Eng. Ind. Aerodyn.*, vol. 158, pp. 1–10, 2016, doi: 10.1016/j.jweia.2016.08.011.

[33]   S. Liu, W. Pan, H. Zhang, X. Cheng, Z. Long, and Q. Chen, "CFD simulations of wind distribution in an urban community with a full-scale geometrical model," *Build. Environ.*, vol. 117, pp. 11–23, 2017, doi: 10.1016/j.buildenv.2017.02.021.

[34]   J. O. Hinze, "Turbulence. McGraw-Hill Publishing Co." New York, 1975.

[35]   S. Starccm, "Fully turbulent flow around a sphere using OpenFOAM," 2012, [Online].

Available: www.OpenFOAM.org.

[36]   A. Zhang, C. Gao, and L. Zhang, "Numerical simulation of the wind field around different building arrangements," *J. Wind Eng. Ind. Aerodyn.*, vol. 93, no. 12, pp. 891–904, 2005, doi: 10.1016/j.jweia.2005.09.001.

[37]   T. Modeling, "Simcenter STAR-CCM + Turbulence Modeling," 2019.

[38]   W. P. Jones and B. E. Launder, "The calculation of low-Reynolds-number phenomena with a two-equation model of turbulence," *Int. J. Heat Mass Transf.*, vol. 16, no. 6, pp. 1119–1130, 1973, doi: 10.1016/0017-9310(73)90125-7.

[39]   B. E. Launder and B. I. Sharma, "Application of the energy-dissipation model of turbulence to the calculation of flow near a spinning disc," *Lett. Heat Mass Transf.*, vol. 1, no. 2, pp. 131–137, 1974, doi: 10.1016/0094-4548(74)90150-7.

[40]   R. N. T. Flows-model, "A New k-e Eddy Viscosity Model for High," no. August, 1994.

[41]   S. Victor and M. Paraschivoiu, "Performance of a Darrieus turbine on the roof of a building," *Trans. Can. Soc. Mech. Eng.*, vol. 42, no. 4, pp. 341–349, 2018, doi: 10.1139/tcsme-2017-0096.

[42]   S. Star-ccm, "Simcenter STAR-CCM + New features and enhancements," 2019.

[43]   A. Thesis, "UNSTEADY AND THREE-DIMENSIONAL CFD SIMULATION OF A DARRIEUS TURBINE ON THE ROOF OF A BUILDING of Mechanical , Industrial and Aerospace Engineering Presented in the Partial Fulfillment of Requirements for the Degree of MASTER OF APPLIED SCIENCE (MECHANICA," no. July, 2017.

[44]   ANSYS, "ANSYS - Turbulence Modelling and the Law of the Wall: Tutorial," *ANSYS User Man.*, pp. 1–48, 2014.

[45]   S. Zhong, J. Li, C. D. Whiteman, X. Bian, and W. Yao, "Climatology of high wind events in the Owens Valley, California," *Mon. Weather Rev.*, 2008, doi: 10.1175/2008MWR2348.1.

[46]   C. Borri and E. Marino, "Winercost 2018 Proceedings," no. March, 2018.

[47]   "Wind & weather statistics Montréal–Dorval Airport - Windfinder."
        https://www.windfinder.com/windstatistics/dorval_lake_saint_louis?utm_source=www.
        windfinder.com&utm_medium=web&utm_campaign=redirect (accessed Jul. 02, 2021).

Appendix 1

Case I, King Street

The energy output in all 4 points from all 8 directions

Table 11: Estimated Energy output at the location of point 1 with the West wind direction

Average Velocity m/s	2	4	6	8	10	12	14
Actual velocity m/s	0.972	1.94	2.92	3.89	4.86	5.83	6.80
Power Watts/m^2	0.564773	4.52	15.25	36.15	70.60	121.99	193.72
Frequency	5.83%	9.22%	9.00%	5.72%	2.43%	0.60%	0.24%
Energy $Wh/_{m^2}$	288	3649	12022	18111	15027	6411	4072

Table 12: Estimated Energy output at the location of point 2 with the West wind direction

Average Velocity m/s	2	4	6	8	10	12	14
Actual velocity m/s	2.8024	5.60	8.41	11.21	14.01	16.81	19.62
Power Watts/m^2	13.53523	108.28	365.45	866.25	1691.90	2923.61	4642.58
Frequency	5.83%	9.22%	9.00%	5.72%	2.43%	0.60%	0.24%
Energy $Wh/_{m^2}$	6912	87456	288121	434055	360152	153664	97605

Table 13: Estimated Energy output at the location of point 3 with the West wind direction

Average Velocity m/s	2	4	6	8	10	12	14
Actual velocity m/s	0.412	0.82	1.24	1.65	2.06	2.47	2.88
Power Watts/m^2	0.04301	0.34	1.16	2.75	5.38	9.29	14.75
Frequency	5.83%	9.22%	9.00%	5.72%	2.43%	0.60%	0.24%
Energy $Wh/_{m^2}$	21	277	915	1379	1144	488	310

Table 14: Estimated Energy output at the location of point 4 with the West wind direction

Average Velocity m/s	2	4	6	8	10	12	14
Actual velocity m/s	0.836	1.67	2.51	3.34	4.18	5.02	5.85

Power Watts/m^2	0.35933	2.87	9.70	23.00	44.92	77.62	123.25
Frequency	5.83%	9.22%	9.00%	5.72%	2.43%	0.60%	0.24%
Energy $Wh/_{m^2}$	183	2321	7648	11523	9561	4079	2591

Table 11, Table 12, Table 13 and Table 14 are showing the Actual velocity and Energy output at each 4 control points while the wind is rising from the West direction, it is observed the due to the location of point 2 and the exposure of this point to the West wind direction, it has the most amount of energy output among the 4 control points at each corner of the rooftop of the building.